

<b>Title:</b>	<b><i>DRAFT- Digital Re-Design of Continuous-Time PLLs</i></b>
<b>Abstract:</b>	<p>The need frequently arises to design a discrete-time digital signal processing (DSP) algorithm that closely mimics a conventional continuous-time phase-locked loop (CTPLL). Similarly, it is often desirable to talk about the DSP implementation in terms of traditional quantities like damping factor and equivalent noise bandwidth. This memorandum examines this interplay between discrete and continuous time systems in the context of the classical continuous-time type-2 PLL. It also provides detailed design formula for implementing CTPLL designs with finite-difference equations for digital implementation.</p> <p><i>For readers who prefer to skip the exhaustive material and jump right to the preferred re-design method, go to Section 7 which develops the bilinear transform method for re-design directly.</i></p>
<b>Date:</b>	2 April 2005
<b>Author:</b>	J.A. Crawford
<b>Ref. No.</b>	U11700

## 1 Introduction

Discrete-time and continuous-time phase-locked loop (DTPLL and CTPLL) implementations are fundamentally different. The behavioral differences between these different systems becomes almost indistinguishable however, as the over-sampling rate (OSR) in the digital signal processing (DSP) is increased. The ratio of sampling rate to the PLL closed-loop unity-gain frequency will be defined in this memorandum as [1]

$$(1) \text{ OSR} = \frac{F_s}{\sqrt{2} \left( \frac{\omega_n}{2\pi} \right)}$$

in which  $F_s$  is the sampling rate in Hz, and  $\omega_n$  is the PLL's natural frequency in radians/s. Although this definition was not formally presented in [1], it is a very

convenient definition because closed-loop unity gain frequency is precisely given by the denominator in (1) for the type-2 CTPLL, and this relationship is independent of the damping factor  $\zeta$ .

For a second-order, type-2 CTPLL, the damping factor and phase margin are closely related by the approximation<sup>1</sup>

$$(2) \zeta \approx 0.01 \phi_{PM\_deg}$$

It is of course no surprise that system stability margin and the time-domain behavior are interconnected, but this is a useful approximation for the discussions that are presented later. We would otherwise lack a simple means to relate a discrete-time system's characteristics back to the CTPLL damping factor equivalent.

The main purposes of this memorandum are:

- To provide a mathematical basis and means to convert the classical second-order type-2 CTPLL into a discrete-time system
- To investigate different metrics of equivalence between CTPLL and DTPLL designs
- To provide the mathematical framework to assist in analyzing other arbitrary designs that may be of interest.

The PLL satisfies a cornucopia of different engineering needs in today's world, and as such it is necessary to at least attempt to capture some of these different perspectives in the discussions that follow. To that end, we will consider the extracted DTPLL designs from several different perspectives including: (i) time-domain response, (ii) frequency-domain closed-loop gain, (iii) equivalent noise bandwidth.

There are many graphical plots contained in this memorandum. This was purposely done in order to enhance readability but it does make this a very lengthy monologue. Conclusions are provided at the end of each major section where appropriate in boxed regions in order that key points are not overlooked or lost.

### 1.1 Continuous-Time and Discrete-Time System Important Relationships

Two equations from [1] (equations 1 and 8) form much of the foundational basis for the technical discussions that follow. The first of these two equations makes use of the Poisson Sum formula to permit the

<sup>1</sup> [4], page 251, equation (8-58)

discrete-time and continuous-time transform descriptions of a system to be translated as

$$(3) \sum_k T_s h(kT_s) \exp(-j2\pi f k T_s) = \sum_m H\left(f \pm \frac{m}{T_s}\right)$$

In (3), the left-hand side is mathematically the z-transform (scaled by  $T_s$ ) of the time-series given by  $h_k = h(kT_s)$  whereas  $H(f)$  is the continuous-time Fourier transform of  $h(t)$ . The sampling rate is  $F_s$  with  $F_s = T_s^{-1}$ . The second equation of interest makes it possible to use the continuous-time Fourier transform of the open-loop gain function to compute the closed-loop frequency-domain description of the sampled control system and is given by

$$(4) H(s) = \frac{G_{OL}(s)}{1 + \frac{1}{T_s} \sum_k G_{OL}\left(s + j\frac{2\pi k}{T_s}\right)}$$

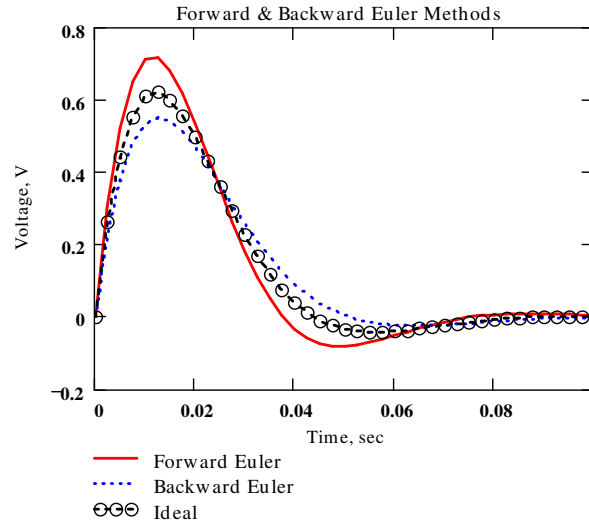
These equations receive substantial consideration in [2] should the interested reader wish to follow the underlying details more rigorously. One of the most attractive features of (4) is that it permits the exact inclusion of sampling in an otherwise continuous-time system without the need of first computing the z-transforms involved. Although we will not exploit this perspective in this memorandum, but it is nonetheless worthy of special note.

Since the CTPLL and DTPLL are not precisely the same particularly for small OSR values, the notion of an “equivalent” DSP redesign of a CTPLL must receive additional definition. The question, “Equivalent how?” must be asked. Different systems will naturally require a different definition of equivalence such as equivalence in:

- Equivalent Noise Bandwidth
- Bandwidth at -3 dB
- Natural Frequency and Damping Factor
- Stability Margin (Gain Peaking)
- Impulse Response

Ultimately, we must decide how the Laplace transform operator  $s$  and the z-transform operator  $z$  are to be related in our redesign methodology. Equivalently, we must decide how differentiation and integration in the time domain will be handled between the continuous-time and discrete-time systems. A glimpse of this issue is offered in Figure 1 where the forward and backward Euler integration methods are compared for the continuous time domain systems which has an impulse response given as

**Figure 1 Comparison Between Forward and Backward Euler Integration Methods**



$$(5) v(t) = \frac{2\zeta}{\sqrt{1-\zeta^2}} e^{-\zeta\omega_n t} \sin\left(\omega_n \sqrt{1-\zeta^2} t\right)$$

for  $t \geq 0$ . The resulting responses are substantially different even for appreciable OSR values as evidenced here. More information is provided in the next section concerning such integration methods.

Finally, a word about system stability is in order. As is true with any numerical simulation work, stability is crucial for achieving any meaningful results. In the context of the material presented in this memorandum, two different forms of stability must be considered. First of all, the underlying numerical integration formulas that are adopted must be in a parameter range where they are themselves stable as discussed in Section 2. Secondly, the design of the DTPLL must itself be stable. The first stability type is easily achieved by using an adequate OSR parameter whereas the second depends upon proper pole-zero placement for the DTPLL design itself. Stability issues need to be considered in context since there are different types of stability that must be considered.

- “Equivalence” between CTPLL and DTPLL is a subjective term that must be precisely quantified.
- Overall stability requires both (i) stability of the underlying numerical integration model and (ii) the system barring any imperfections in the numerical integration

## 2 s- and z-Operators in Terms of Integration Formulas

It is very convenient to think about the Laplace transform  $s$  as a mathematical operator that is to be replaced by a discrete time operator in terms of  $z$  which is the unit-time element of  $z$ -transform theory. It is desirable that the adopted discrete time operator be both simple and accurate. The accuracy issue is particularly important if the OSR parameter is small.

In this section, we will introduce 4 different discrete-time methods for approximating the continuous-time Laplace transform operator  $s$ . These methods will subsequently be used to redesign the CTPLL into a discrete-time system implementation. A fifth technique is developed at the beginning of Section 3 which is based upon an impulse-invariant perspective.

All of the integration formulas that we will consider in this memorandum are documented in numerical method textbooks. Two references that provide extensive treatment of this subject are [2] and [3].

### 2.1 Forward Euler Integration

The Forward Euler (FE) integration formula is the most simple algorithm that we can choose to employ. It is also the most inaccurate and potentially unstable algorithm that we will consider. This formula originates from approximating  $z$  as

$$(6) \quad z = e^{sT} \approx 1 + sT$$

from which we may write

$$(7) \quad s \approx \frac{z-1}{T}$$

In the discrete time domain, this is equivalent to defining the time derivative of a signal  $x(t)$  as

$$(8) \quad \dot{x}_n = \frac{x_{n+1} - x_n}{T}$$

which leads to

$$(9) \quad x_{n+1} = x_n + T \dot{x}_n$$

In the context of the first-order initial value problem in which  $dx/dt = -\lambda x(t)$ , the discrete-time equation becomes

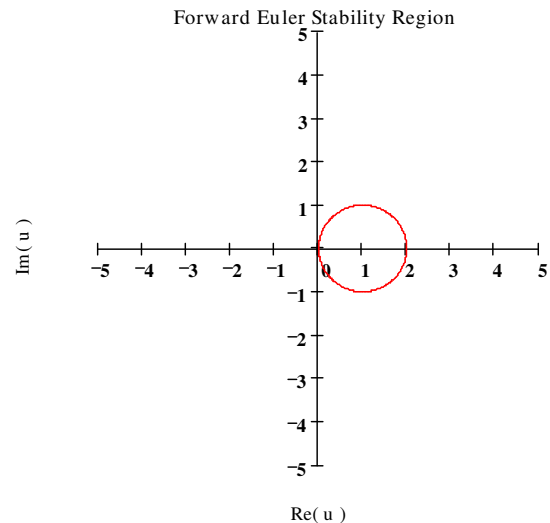
$$(10) \quad x_{n+1} = (1 - \lambda T)x_n$$

and the eigenvalue region for which the formula remains stable is that for which

$$(11) \quad |1 - \lambda T| < 1$$

The corresponding stability region for this integration formula is shown in Figure 2. Compared to the methods that follow, this stability region is dramatically smaller than that exhibited by the other methods. This small stability region forces the implementation to utilize a high OSR value in order to achieve a reasonable match with the behavior of the CTPLL. Although the FE method is rather intuitive and consequently frequently adopted, its use should be strongly discouraged unless the designer is well aware of its short-comings.

**Figure 2 Stability Region For The Forward Euler Method Is The Interior of Circle ( $u = \lambda T$ )**



### 2.2 Backward Euler Integration

The Backward Euler (BE) integration formula is also a first-order method similar to the FE formula, but it is an **implicit** integration formula rather than an **explicit** one like the FE method. As is true of most implicit integration formulas, they offer superior stability as compared with explicit formulas of similar complexity. This formula originates from approximating  $z^{-1}$  as

$$(12) \quad z^{-1} = e^{-sT} \approx 1 - sT$$

from which we may write

$$(13) s \approx \frac{1}{T} \frac{z-1}{z}$$

In the discrete time domain, this is equivalent to defining the time derivative of a signal  $x$  as

$$(14) \dot{x}_{n+1} = \frac{x_{n+1} - x_n}{T}$$

which leads to

$$(15) x_{n+1} = x_n + T \dot{x}_{n+1}$$

In the context of the first-order initial value problem in which  $dx/dt = -\lambda x(t)$ , the discrete-time equation becomes

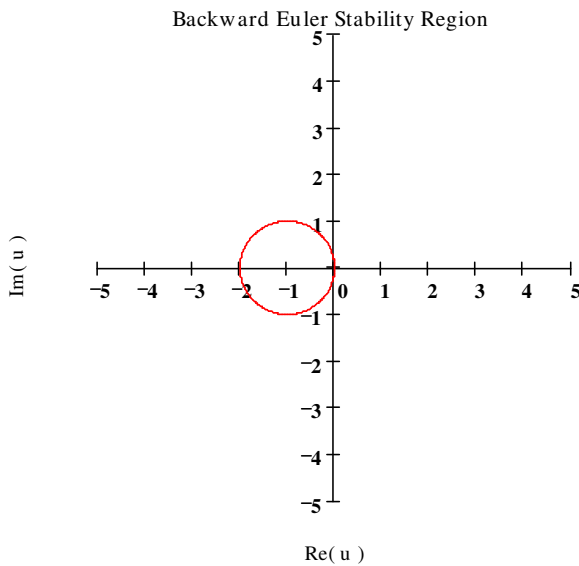
$$(16) x_{n+1} = (1 + \lambda T)^{-1} x_n$$

and the eigenvalue region for which the formula remains stable is that for which

$$(17) |1 + \lambda T|^{-1} > 1$$

The corresponding stability region for this integration formula is shown in Figure 3.

**Figure 3 Stability Region For The Backward Euler Method Is The Exterior Of The Circle ( $u = \lambda T$ )**



The stability region for the BE method is dramatically larger than the FE method. As far as first-order methods are concerned, the BE method is highly

recommended.

### 2.3 Trapezoidal Integration

Trapezoidal integration is another implicit integration formula which is actually the well-known bilinear transform method in disguise. It is based upon approximating  $z^{-1}$  as

$$(18) z^{-1} = e^{-sT} \approx \frac{1 - \frac{sT}{2}}{1 + \frac{sT}{2}}$$

from which we may write

$$(19) s \approx \frac{2}{T} \frac{z-1}{z+1}$$

In the discrete time domain, this is equivalent to writing

$$(20) x_{n+1} = x_n + \frac{T}{2} \left( \dot{x}_{n+1} + \dot{x}_n \right)$$

In the context of the first-order initial value problem in which  $dx/dt = -\lambda x(t)$ , the discrete-time equation becomes

$$(21) x_{n+1} = \left( \frac{1 - \frac{T\lambda}{2}}{1 + \frac{T\lambda}{2}} \right) x_n$$

and the eigenvalue region for which the formula remains stable is that for which

$$(22) \left| \frac{1 - \frac{T\lambda}{2}}{1 + \frac{T\lambda}{2}} \right| < 1$$

The trapezoidal method simply requires that  $\text{Re}(\lambda) > 0$  for stability. This is a pleasing result since it insures that the output is bounded so long as the input is bounded.

The stability region for the BT method is the entire left-hand plane. As long as the input signal is bounded, so is the output.

## 2.4 Second-Order Gear Integration

The last implicit integration formula that we will consider here is the 2<sup>nd</sup>-order Gear algorithm. This formula class is particularly well suited for stiff differential equations (i.e., equations having widely separated eigenvalues). The associated discrete time difference equation associated with this method is given by

$$(23) x_{n+1} = \frac{4}{3}x_n - \frac{1}{3}x_{n-1} + \frac{2}{3}T \dot{x}_{n+1}$$

Rearranging terms, this becomes

$$(24) \dot{x}_{n+1} = \frac{3}{2T} \left[ x_{n+1} - \frac{4}{3}x_n + \frac{1}{3}x_{n-1} \right]$$

From this result, we may conclude that the Laplace transform operator  $s$  (viewed as a differentiation operator) for the 2<sup>nd</sup>-order Gear Method is given by

$$(25) s = \frac{3}{2T} \left( 1 - \frac{4}{3}z^{-1} + \frac{1}{3}z^{-2} \right)$$

In the context of the first-order initial value problem in which  $dx/dt = -\lambda x(t)$ , the region of absolute stability for this method is described by the exterior region of the curve given by<sup>2</sup>

$$(26) \sigma(\theta) = -\frac{3}{2} + 2e^{-j\theta} - \frac{1}{2}e^{-j2\theta}$$

This stability region is plotted in Figure 4.

## 2.5 Summary

A number of the more important points from this section are summarized below.

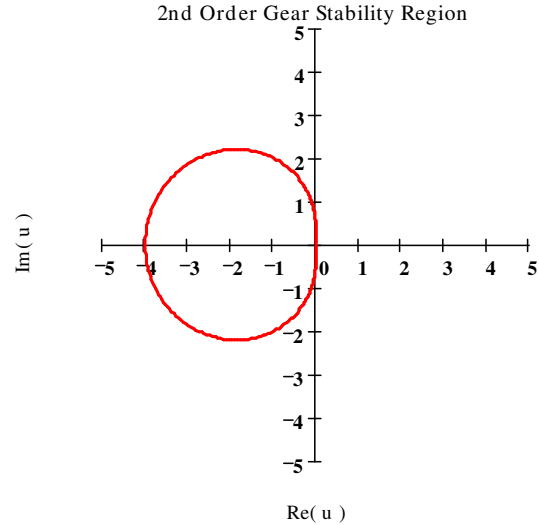
- Implicit integration methods (e.g., Backward Euler, Trapezoidal, and Gear) are much preferred over explicit methods.
- Although simple to implement, the Forward Euler method should be avoided.
- The Trapezoidal integration formula is stable for all inputs that are bounded. It is equivalent to the well-known bilinear transform method.

With these basic concepts now in hand, we can consider the CTPLL redesign question in the realm

<sup>2</sup> From [3], equ. (13-70)

of the integration formulas just discussed.

**Figure 4 Stability Region For The 2<sup>nd</sup>-Order Gear Method Is The Exterior Of The Plotted Region ( $u = \lambda T$ )**



## 3 CTPLL Redesign

If our intent is to convert a CTPLL into a DTPLL, we must have a technique or formula that permits us to move between the two respective domains accordingly. Quite frequently, this is done in a fairly ad-hoc manner. Adding additional rigor and insight into this specific issue is one of the main purposes of this paper. The integration formulas of the previous section provide the needed recipes for moving between the continuous-time and discrete-time domains.

### 3.1 Basic Type-2 CTPLL

Our focus in this memorandum is limited to the basic type-2 CTPLL because it is a heavily utilized architecture with which most engineers have some familiarity. The open-loop gain function for the basic continuous-time 2<sup>nd</sup>-order type-2<sup>3</sup> PLL is given by

$$(27) G_{ol}(s) = \left( \frac{\omega_n}{s} \right)^2 \left( 1 + \frac{2\zeta}{\omega_n} s \right)$$

where  $\omega_n$  is the natural frequency in radians/second and  $\zeta$  is the damping factor.

There are two closed-loop transfer functions that are primarily of interest regarding the CTPLL. The

<sup>3</sup> loop "type" refers to the number of ideal poles in the transfer function

first involves the transfer function between the output phase and the input phase. It has an expected lowpass filter characteristic that is given by

$$(28) H_1(s) = \frac{G_{ol}(s)}{1+G_{ol}(s)} = \frac{\omega_n^2 \left(1 + \frac{2\zeta}{\omega_n} s\right)}{s^2 + 2\zeta\omega_n s + \omega_n^2}$$

The second transfer function is more relevant to continuous-time systems in which the PLL's voltage-control oscillator (VCO) has imperfect phase noise performance. This transfer function pertains to the relationship between the output phase from the (closed-loop) PLL and any phase perturbation introduced by the VCO acting stand-alone. We will not be concerned with this transfer function in our redesign efforts, but this transfer function is included here for completeness. It is given by

$$(29) H_2(s) = \frac{1}{1+G_{ol}(s)} = \frac{s^2}{s^2 + 2\zeta\omega_n s + \omega_n^2}$$

This transfer function is obviously highpass in nature.

An example plot of  $H_1(\cdot)$  is provided in Figure 5 for the case where  $\omega_n / (2\pi) = 10$  kHz and  $\zeta = 0.75$ . A number of helpful equations that express important quantities like 3 dB bandwidth, maximum gain-peaking, etc. can be found in [1], and these are provided in Section 12 for easy reference. As mentioned in the introduction segment, matching open-loop gain characteristics between the continuous-time and discrete-time systems is but one possible metric of equivalence that may be pursued in the redesign effort.

## 4 CTPLL Redesign Using Impulse Response Invariance

The first redesign method that we will consider does not rely upon an explicit mapping of the Laplace transform  $s$  to the  $z$ -domain, and we consider this method here. This method is used extensively in Chapter 5 of [2] in order to include sampling effects in continuous-time but sampled PLLs. We will necessarily have to modify the details somewhat in order to fit within the present range of our discussions.

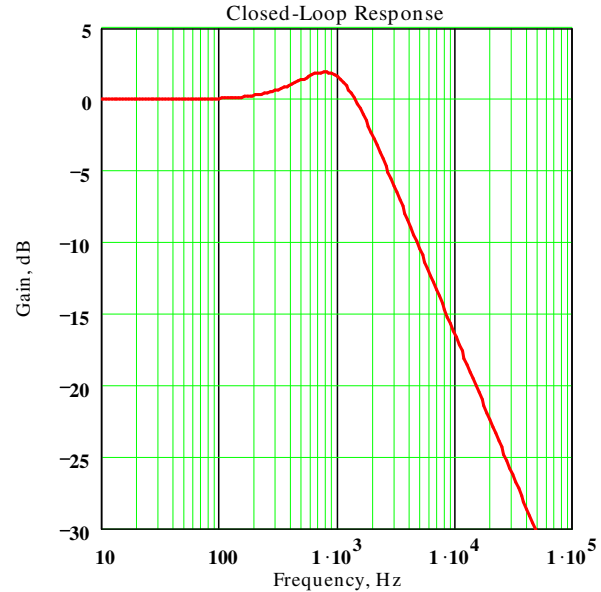
In order to perform the redesign task, we normally must be able to separate out the presence of the loop filter function and the frequency-controlled oscillator. We are therefore forced to focus on the open-loop gain function (27) rather than the closed-loop  $H_1$  function (28). If we start with (27) and take the

inverse Laplace transform, we obtain the time-domain function given by

$$(30) h(t) = \omega_n^2 t + 2\zeta\omega_n u(t)$$

in which  $u(t)$  represents the unit-step function. If we then take the  $z$ -transform of (30) directly, we obtain

**Figure 5 Closed-Loop Gain Characteristic for CTPLL with 10 kHz Natural Frequency and 0.75 Damping Factor**



$$(31) H(z) = \omega_n^2 \frac{Tz}{(z-1)^2} + \frac{2\zeta\omega_n z}{z-1}$$

$$= \left[ \frac{\frac{2\zeta}{\omega_n} z + \left(T - \frac{2\zeta}{\omega_n}\right)}{z-1} \right] \omega_n^2 \frac{z}{z-1}$$

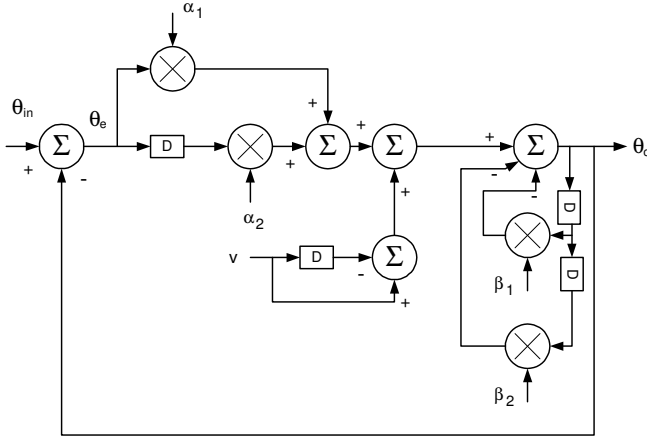
In moving from the continuous-time Laplace domain to the discrete-time  $z$ -domain, from (3) we must include another factor of  $T$  since the input continuous-time function  $\theta(t)$  and its sampled form  $\theta^*(t)$  are approximately related by a scaling factor of  $T$  as  $\text{Laplace}\{\theta^*(t)\} \cong T^{-1}\theta(s)$ . Once this factor has been taken into account, the discrete-time redesign of the CTPLL appears as shown in Figure 6. In this figure, the parameters are defined as follows:

$$(32) \begin{aligned} \alpha_1 &= ac \\ \alpha_2 &= bc \\ \beta_1 &= bc - 2 \\ \beta_2 &= 1 \end{aligned}$$

$$(33) \begin{aligned} a &= \frac{2\zeta}{\omega_n} \\ b &= T - \frac{2\zeta}{\omega_n} \\ c &= \omega_n^2 T \end{aligned}$$

with

**Figure 6 CTPLL Redesign Using Impulse Response Invariance**



Normally, any digital implementation of the DTPLL would involve additional registers and delays compared to what is shown in Figure 6 in order to make it more realizable, but a brief look at the additional delay case is delayed until Section 4.4.

If we follow through with  $H(z)$  as defined by (31) and form the closed-loop transfer function that is equivalent to (28), we obtain

$$(34) H_1(z) = \frac{acz^2 + bcz}{(1+ac) \left[ z^2 + z \left( \frac{cb-2}{1+ac} \right) + \frac{1}{1+ac} \right]}$$

This result can be used to easily compare the frequency-domain behavior of the continuous-time system versus the so-called redesigned discrete-time system.

The transient response of the DTPLL is described by the second-order difference equation given by

$$(35) \theta_{out_{k+1}} = \frac{v_k - v_{k-1} + ac\theta_{in_k} + bc\theta_{in_{k-1}}}{1+ac} - \frac{(bc-2)\theta_{out_{k-1}} + \theta_{out_{k-2}}}{1+ac}$$

in which  $v_k$  represents any applied tunable oscillator control voltage (like that corresponding to a step-frequency change), and  $\theta_{in_k}$  represents any phase sequence that may be applied at the PLL input. The relationship between  $v$  and the applied frequency change is given by  $v = 2\pi F_{step} T$ . This formula is evaluated for several example cases in Section 4.2.

## 4.1 Closed-Loop Stability

The closed-loop stability of the DTPLL described by (35) can be determined by computing the poles of the characteristic equation which corresponds to the denominator polynomial in (34). Stability can also be examined by computing the gain and phase behavior of the open-loop gain function  $H(z)$  given by (31). A little bit of algebra reveals that the poles for the DTPLL's characteristic equation are given by

$$(36) \begin{aligned} r_1 &= -\frac{w_1}{2} \left[ 1 + \sqrt{1 - \frac{4w_2}{w_1^2}} \right] \\ r_2 &= -\frac{w_1}{2} \left[ 1 - \sqrt{1 - \frac{4w_2}{w_1^2}} \right] \end{aligned}$$

in which

$$(37) \begin{aligned} w_1 &= \frac{bc-2}{1+ac} \\ w_2 &= \frac{1}{1+ac} \end{aligned}$$

DTPLL stability is of course crucial for any system that is designed. The root-locus techniques which would make use of these results are basic control theory concepts that are addressed in most textbooks.

There are two basic ways in which this type of DTPLL can be unstable. In the first way, the DTPLL is simply designed with a damping factor  $\zeta$  which is too small. A stable DTPLL case is shown in Figure 7 whereas a DTPLL suffering from insufficient damping factor is shown in Figure 8. The second way in which the DTPLL can become unstable is to employ an insufficient sampling rate compared to the DTPLL bandwidth being used. This situation is shown in Figure 9. In one case, phase margin is completely insufficient whereas in the other, the gain margin is completely insufficient.

**Figure 7 Open-Loop Plots for DTPLL Under Stable Conditions (Gain Margin= 16.16 dB)**

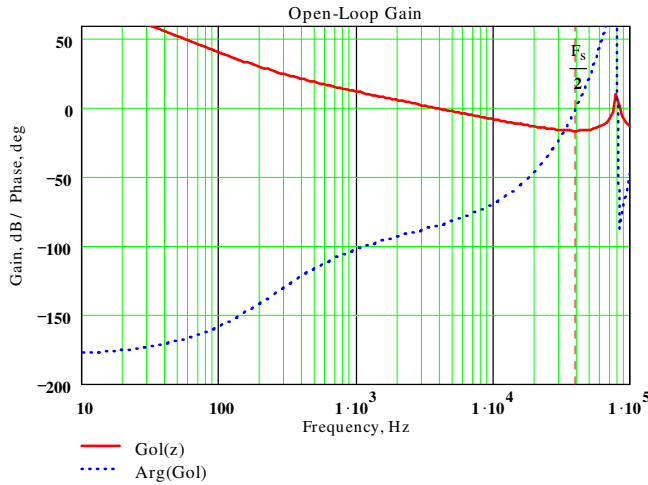


**Figure 8 DTPLL Almost Unstable Case with  $\zeta= 0.01$ . Gain Margin= 62.4 dB Whereas Phase Margin= 1.145°**

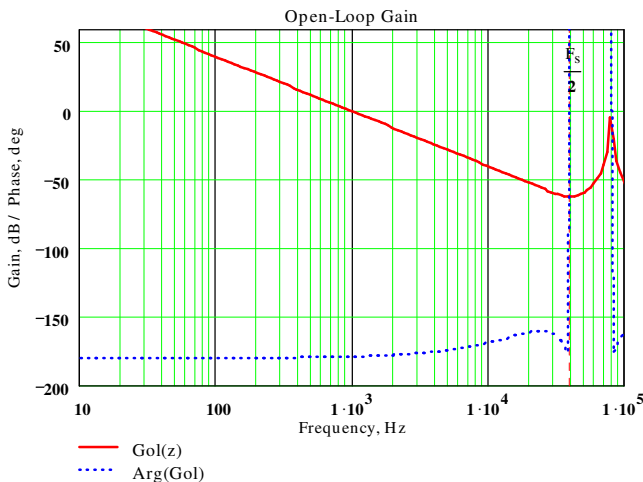
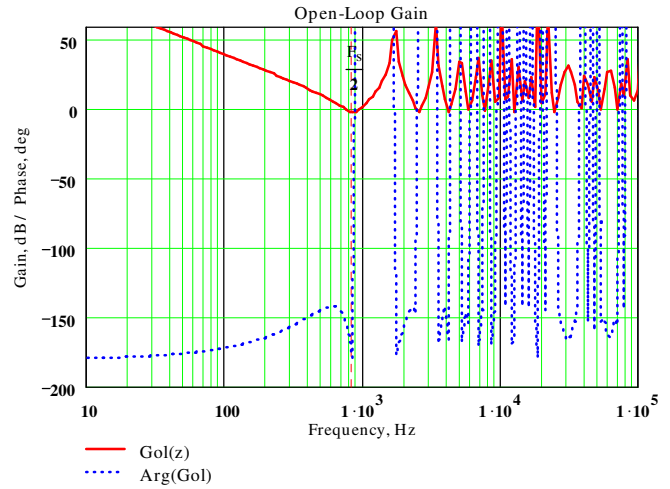


**Figure 9 DTPLL Almost Unstable Case with  $\zeta= 0.707$ . Gain Margin= 1.916 dB and Phase Margin= 26.04°**



When it comes to stability, both gain margin and phase margin must be considered in the general case. As shown in Section 4.4, the inclusion of even two additional unit-delay elements dramatically affects the step-frequency response and the underlying stability margins. Without specific attention to the “additional-delay” issue, this can frequently be a source of significant departure between realized and desired performance. Suffice to say that stability is a very important question which must be addressed before attacking the finer points of DTPLL design offered in this paper.

Always be sure to compute the gain and phase margin for any DTPLL, being careful to include **all** time delays that may be present in the system.

## 4.2 Step-Frequency Response Behavior

The finite difference equation (35) can be used to compute the time-domain DTPLL output phase response to a step-frequency error. The ideal step-frequency response for the CTPLL is given by

$$(38) \theta_o(t) \Big|_{F_{step}} = \frac{2\pi F_{step}}{\omega_n \sqrt{1-\zeta^2}} e^{-\zeta\omega_n t} \sin\left(\omega_n \sqrt{1-\zeta^2} t\right)$$

We will next compare the ideal CTPLL time-domain response with that of the DTPLL for several different OSR values. In all cases, the CTPLL parameters are as follows:

$$(39) \frac{\omega_n}{2\pi} = 1 \text{ kHz}$$

$$\zeta = 0.707$$

The frequency step size employed is 1 kHz. Output phase versus time for the DTPLL and CTPLL are shown in Figure 10 through Figure 13. Obviously, the DTPLL and CTPLL become identical as the OSR is increased. An OSR value between 7 and 14 captures most of the CTPLL characteristic nicely.

*All CTPLL and DTPLL cases considered in this paper assume the basic loop parameters given by (39) and the transient analysis always involves a step-frequency change of 1 kHz.*

**Figure 10 DTPLL Transient Response for Sampling Rate= 3 kHz (OSR= 2.12)**

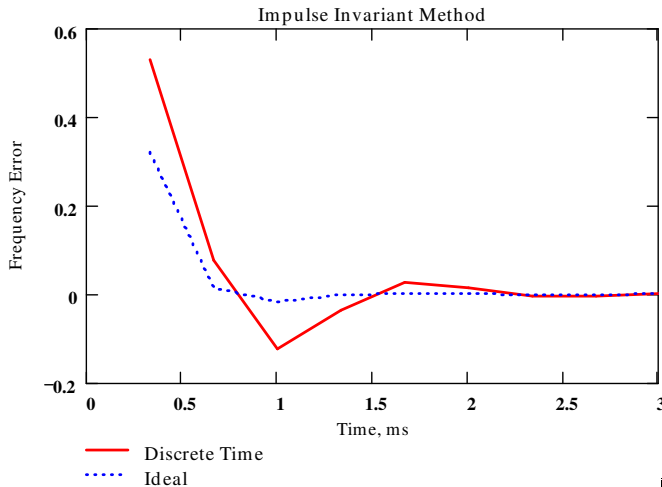


**Figure 11 DTPLL Transient Response for Sampling Rate= 5 kHz (OSR= 3.54)**

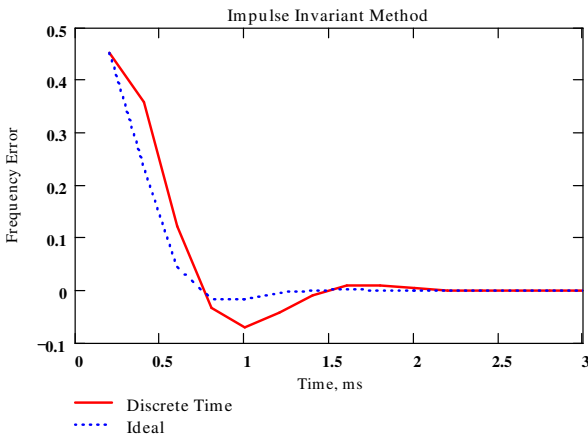


**Figure 12 DTPLL Transient Response for Sampling Rate= 10 kHz (OSR= 7.07)**

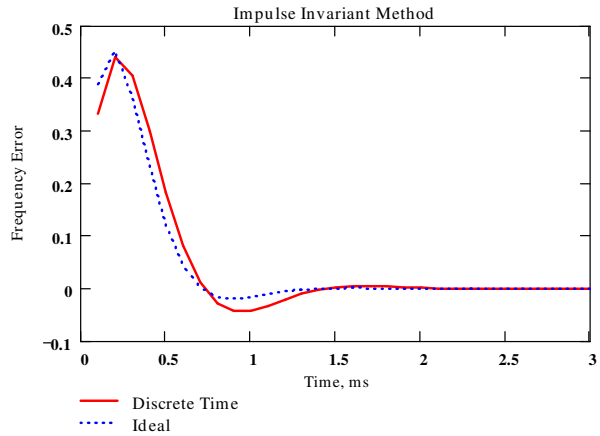
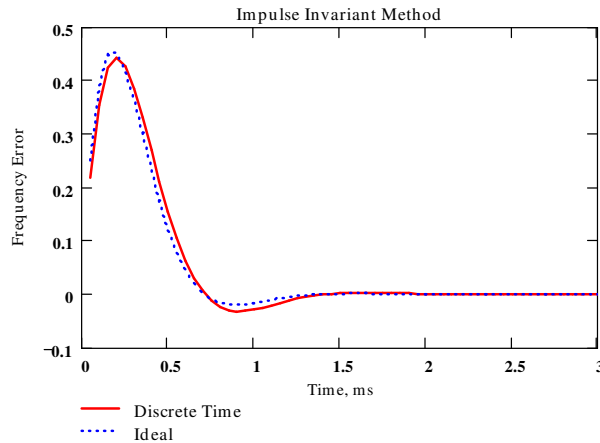


**Figure 13 DTPLL Transient Response for Sampling Rate= 20 kHz (OSR= 14.14)**



In the context of step-frequency response for a damping factor of 0.707, an OSR value between 7 and 14 behaves very closely to the continuous-time system.

### 4.3 Closed-Loop Gain Characteristic

The frequency domain is often a more convenient domain in which to evaluate and assess loop stability issues. Poor loop stability always shows up as excessive “gain peaking” in the closed-loop transfer functions.

Equation (31) is the open-loop gain for the impulse-invariant case when no additional unit-delays are included to facilitate easier implementation. It is a simple matter of course to include an additional factor of  $z^{-m}$  in (31) when  $m$  additional unit-delay elements are present to ease implementation issues. It is a simple matter to construct the resulting  $H_1$  open-loop

gain function as

$$(40) H_1(z) = \frac{H(z)z^{-m}}{1 + H(z)z^{-m}}$$

The closed-loop gain function is examined versus the OSR parameter in Figure 14 through Figure 18 for the  $m=0$  case, and in Section 4.4 for the additional delay case of  $m=2$ .

**Figure 14 Closed-Loop Gain for DTPLL for  $m=0$  with  $F_s=3$  kHz (OSR= 2.121)**

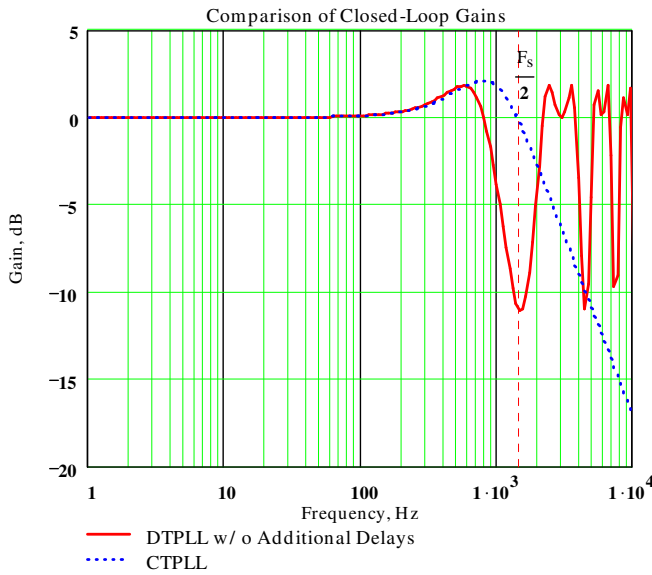


**Figure 15 Closed-Loop Gain for DTPLL for  $m=0$  with  $F_s=5$  kHz (OSR= 3.536)**

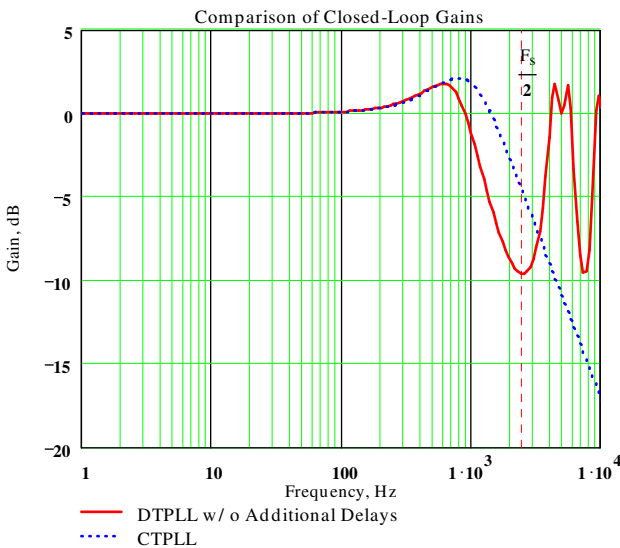


**Figure 16 Closed-Loop Gain for DTPLL for  $m=0$  with  $F_s=10$  kHz (OSR= 7.071)**

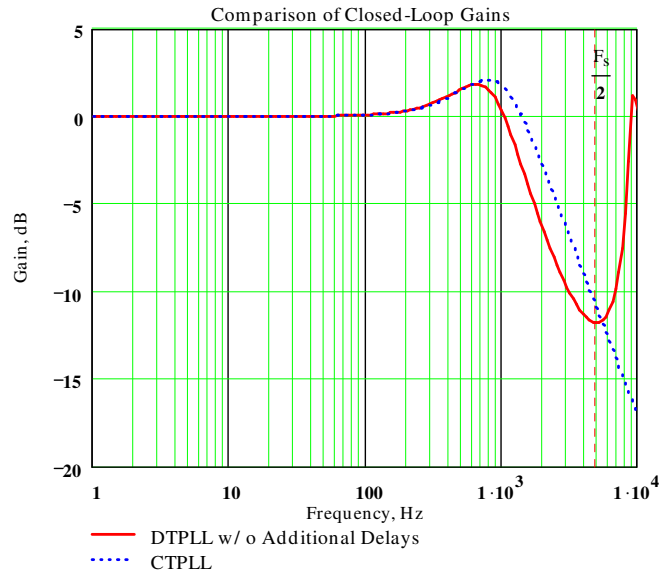
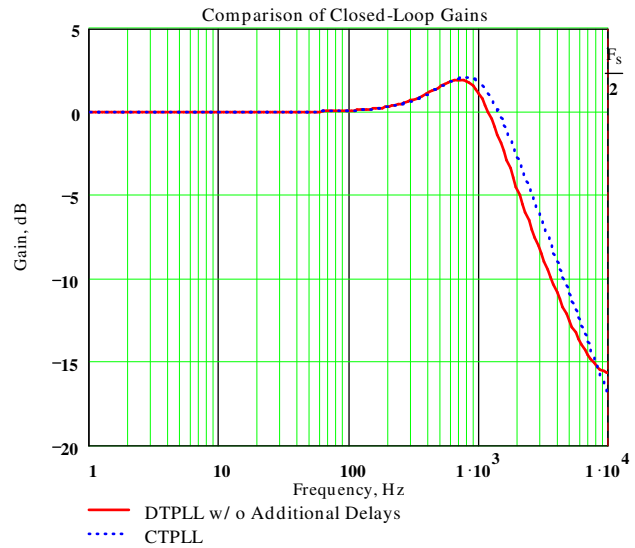


**Figure 17 Closed-Loop Gain for DTPLL for  $m=0$  with  $F_s=20$  kHz (OSR= 14.142)**



Only a small amount of additional gain-peaking is shown in the previous figures. In general, this DTPLL configuration is very well behaved in the frequency domain down to fairly small OSR values as we would expect based upon the step-frequency error responses that we have already seen. The amount of gain peaking versus key loop parameters is shown for this DTPLL in Figure 19. Once additional unit-delays are introduced into the DTPLL implementation however, the stability picture is dramatically altered as discussed later in Section 4.4.

**Figure 18 Closed-Loop Gain for DTPLL for m=0 with  $F_s = 50$  kHz (OSR= 35.355)**

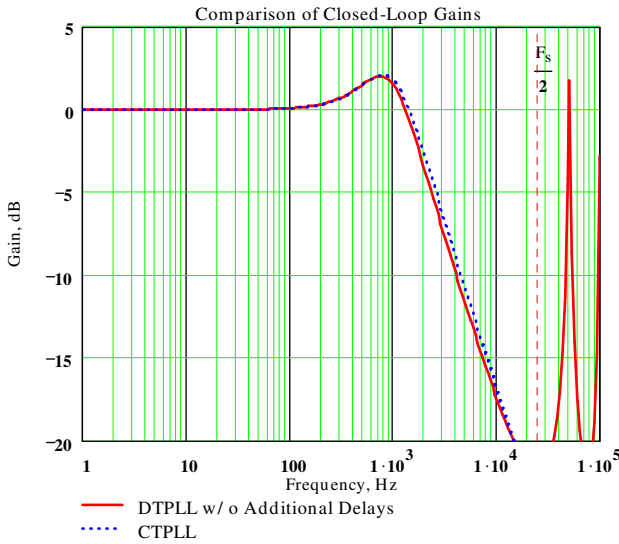
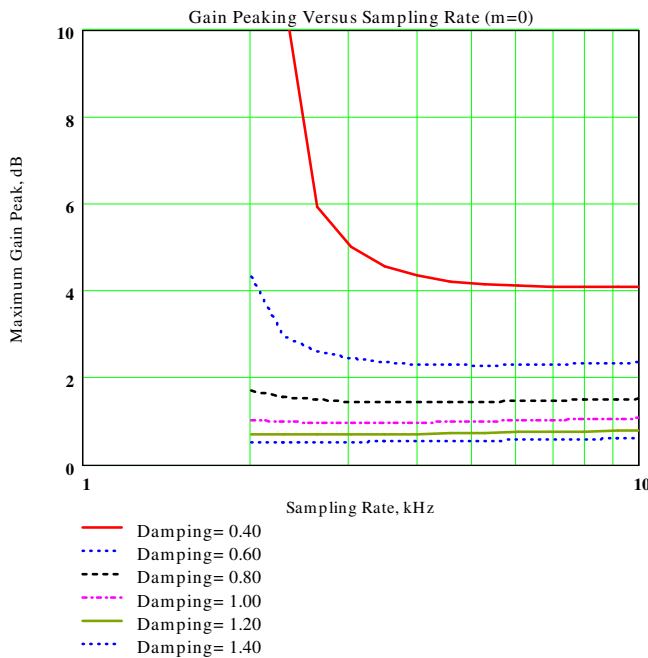


**Figure 19 Closed-Loop Maximum Gain Peaking Versus Sampling Rate and Damping Factor (No Extra Delays; m=0)**

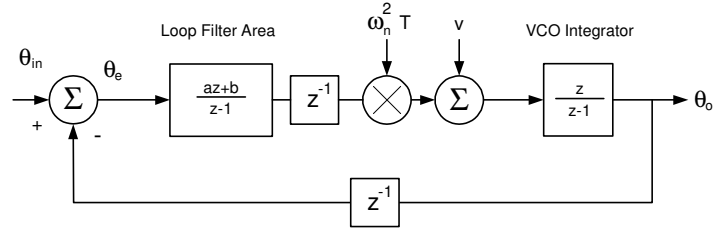


### 4.4 Implementation With Additional Delay Elements

It is a simple matter to insert additional unit-delays in the discrete time equation (31) in order to make the digital design easier to implement as shown in Figure 20. In terms of the open-loop gain function that we had earlier in (31), it must only be augmented

with an additional factor of  $z^{-2}$  since the location of these delays in Figure 20 does not matter as far as it is concerned.

**Figure 20 DTPLL With Additional Delay Elements Included For Easier Implementation**



For small OSR values, the presence of the two additional delay elements results in substantial additional phase shift within the control system which impacts stability. The frequency domain analysis is based upon (40) whereas the finite difference equation for this system is given by

$$(41) \quad \begin{aligned} \theta_{out_k} &= ac \theta_{in_k} + bc \theta_{in_{k-1}} + v_k - v_{k-1} + \\ &2\theta_{out_{k-1}} - (1+ac)\theta_{out_{k-2}} - bc \theta_{out_{k-3}} \end{aligned}$$

Example step-frequency transient responses along with the frequency-domain closed-loop gain behavior are shown for a number of different sampling rates in the figures that immediately follow.

**Figure 21 DTPLL Transient Response with  $F_s = 15$  kHz (OSR= 10.607, m=2)**

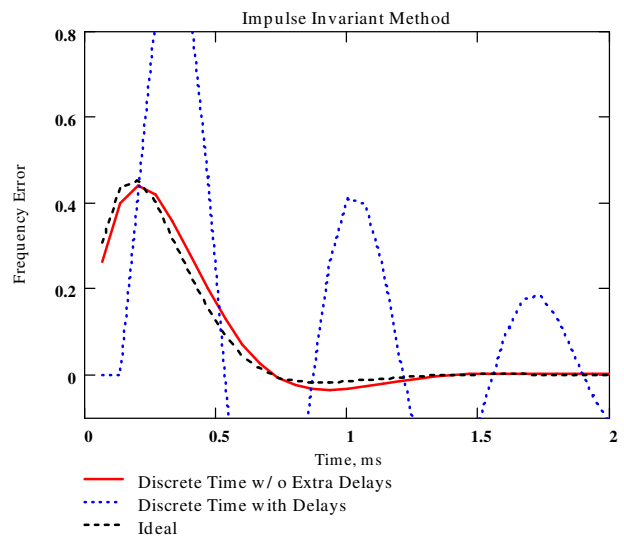


Figure 22 Closed-Loop Gain Corresponding to Figure 21

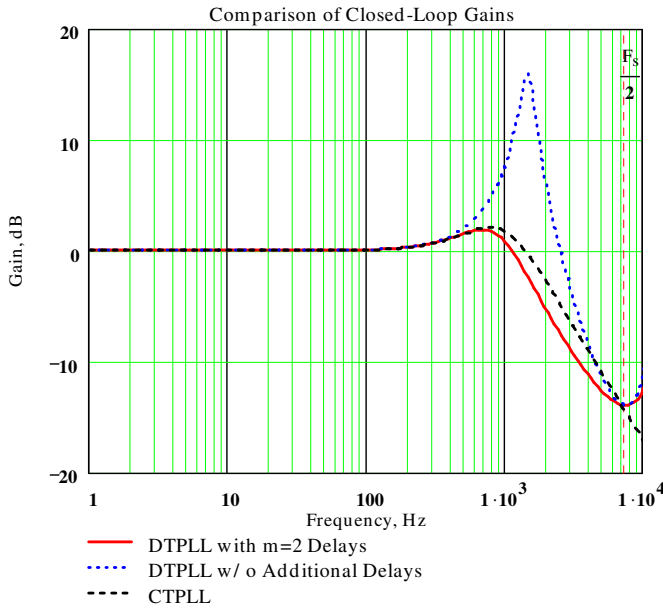


Figure 24 Closed-Loop Gain Corresponding to Figure 23

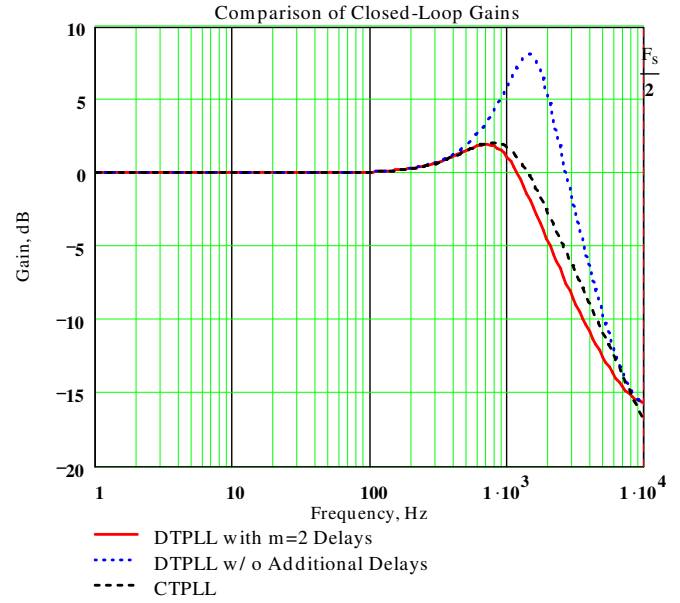


Figure 23 DTPLL Transient Response with  $F_s = 20$  kHz (OSR= 14.142, m=2)

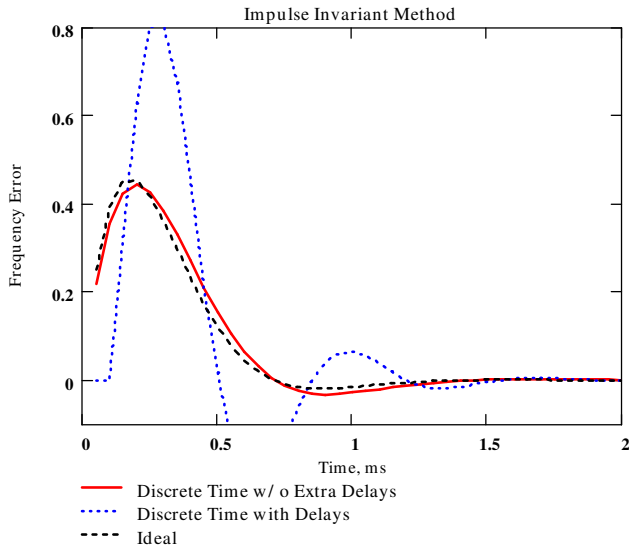


Figure 25 DTPLL Transient Response with  $F_s = 30$  kHz (OSR= 21.213, m=2)

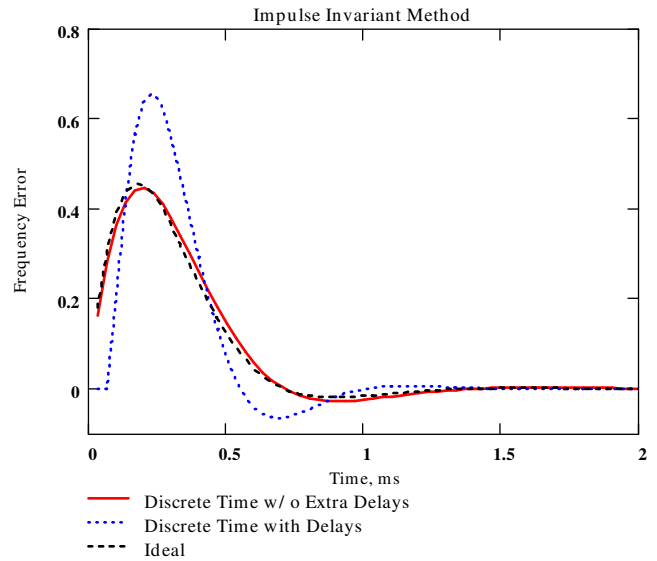


Figure 26 Closed-Loop Gain Corresponding to Figure 25

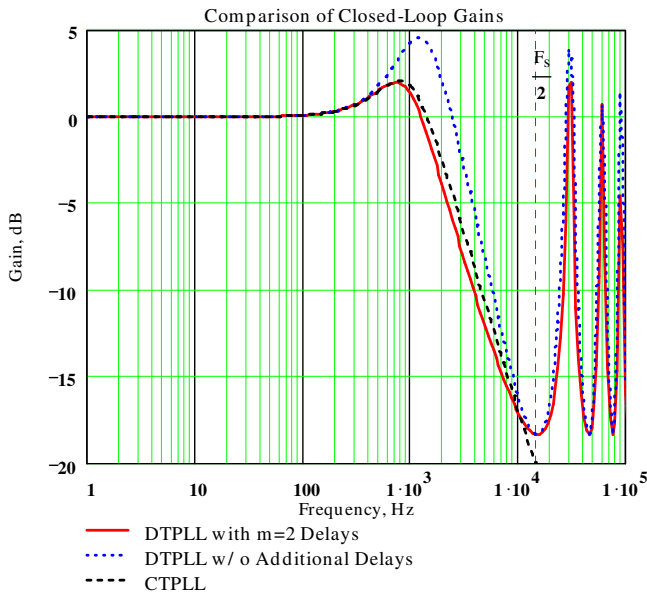


Figure 28 Closed-Loop Gain Corresponding to Figure 27

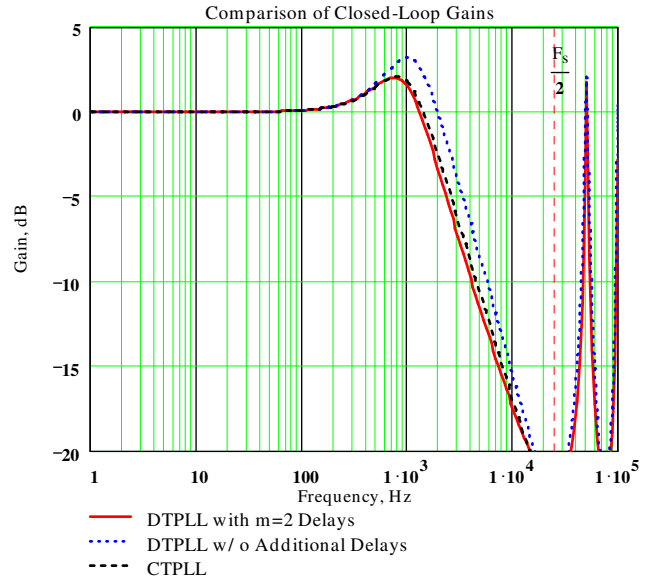


Figure 27 DTPLL Transient Response with  $F_s = 50$  kHz (OSR= 35.355, m=2)

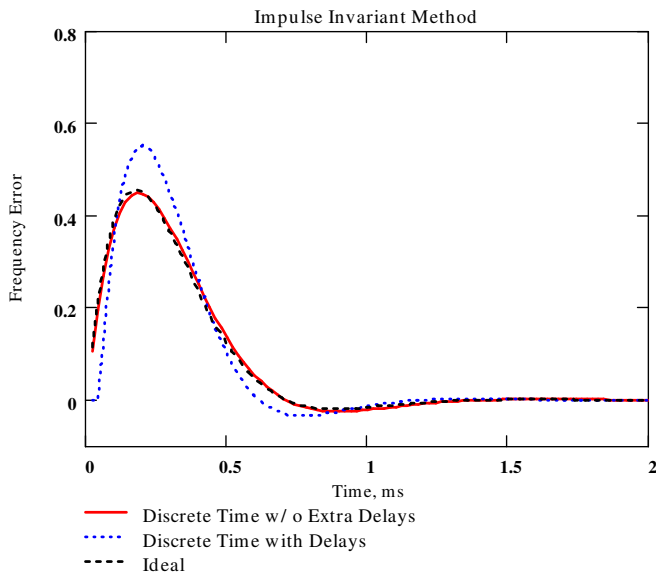
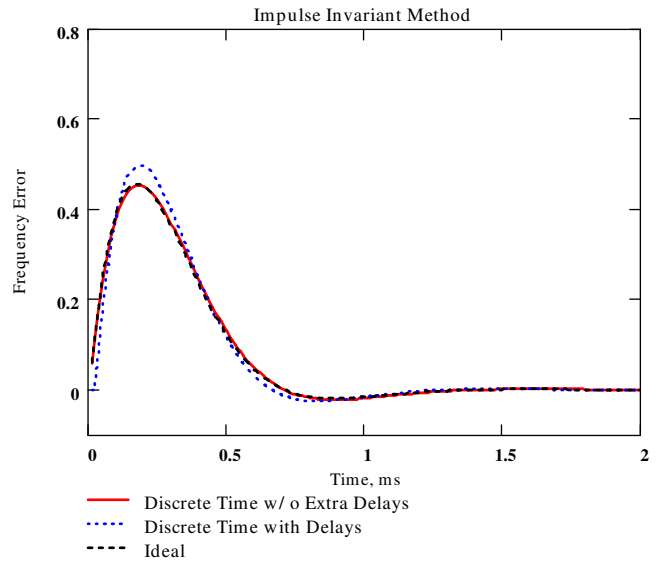
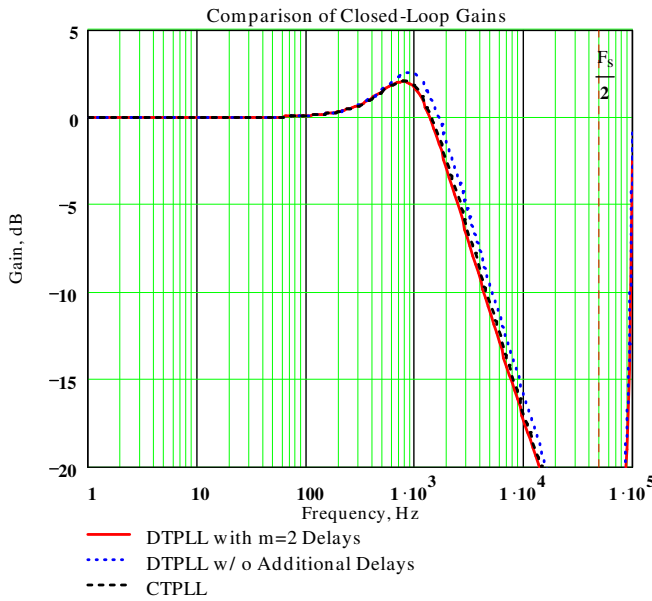


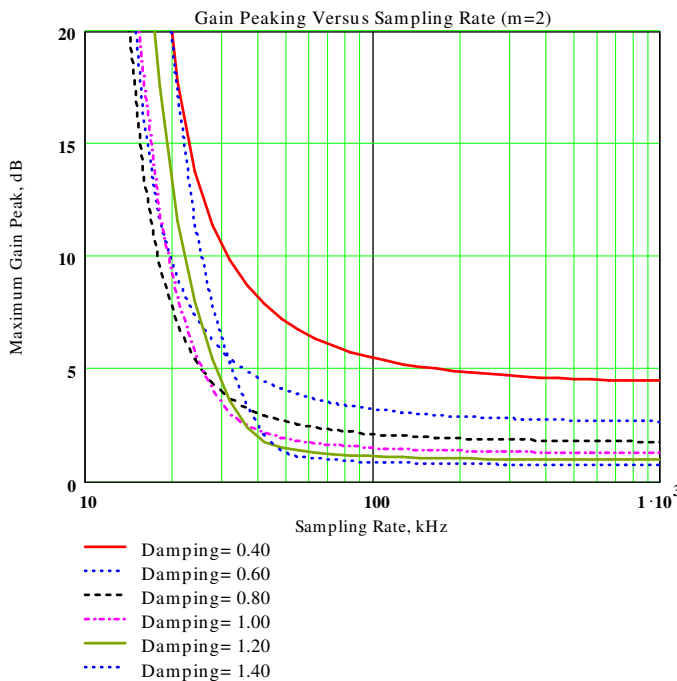
Figure 29 DTPLL Transient Response with  $F_s = 100$  kHz (OSR= 70.711, m=2)



**Figure 30 Closed-Loop Gain Corresponding to Figure 29**



**Figure 31 Closed-Loop Maximum Gain Peaking Versus Sampling Rate and Damping Factor (With Extra Delays; m=2)**



Based upon the prior figures, we fully expect that the amount of gain peaking is much more severe for the m=2 case than for the ideal m=0 case in (40), and this is indeed the case. The gain-peaking plot for the m=2 case that corresponds to Figure 19 for the m=0 case is provided in Figure 31. As shown there,

substantially higher OSR values are required in order to have the same degree of gain peaking present for any specific choice of  $\omega_n$  and  $\zeta$ .

Substantially higher OSR values are required for the m=2 case in order to have the same degree of gain peaking as for the m=0 case.

### 4.5 Equivalent Noise Bandwidth

Calculation of the equivalent noise bandwidth is of course only sensible for strictly stable systems. Given the closed-loop gain function  $H_1(z)$ , the equivalent noise bandwidth can be computed as

$$(42) \quad BW = \int_{\frac{F_s}{2}}^{F_s} |H_1(e^{j2\pi f T_s})|^2 df$$

assuming that the gain  $|H_1(1)| = 1$ . Gain-peaking can significantly increase the equivalent noise bandwidth of the system and this is a major consideration in receiving or tracking type applications. Gain-peaking can be equally undesirable in transmitter-like applications as well. The equivalent noise bandwidth for the m=0 and m=2 DTPLL cases are shown in Figure 32 and Figure 33 respectively. The latter case clearly displays a substantially more problematic equivalent noise bandwidth behavior owing to the greater instability for the m=2 systems.

**Figure 32 Equivalent Noise Bandwidth Versus Sampling Rate and Damping Factor for Impulse-Invariant DTPLL (m=0)**

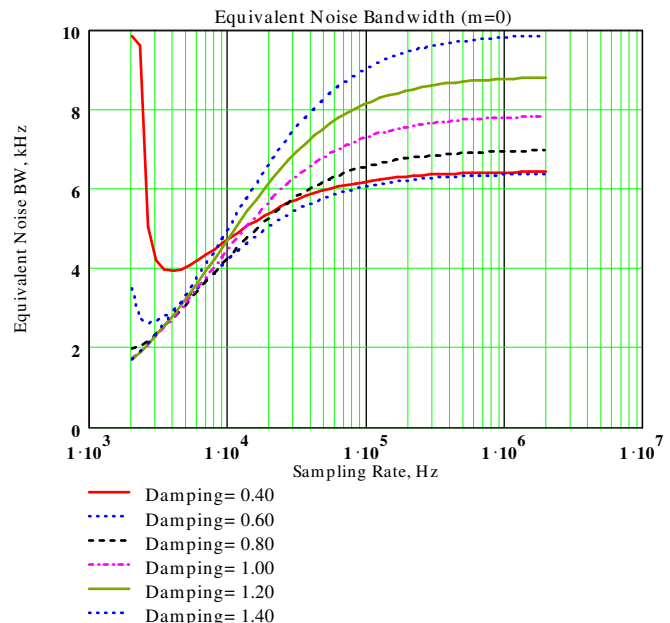
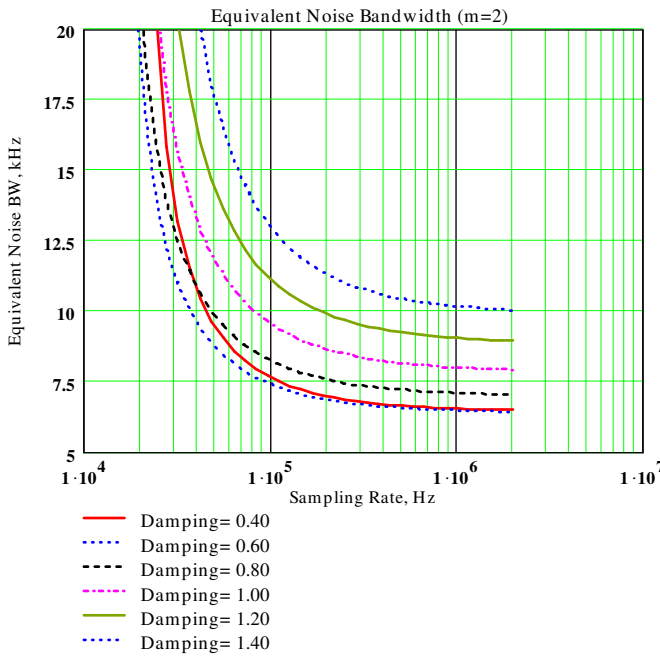


**Figure 33 Equivalent Noise Bandwidth Versus Sampling Rate and Damping Factor for Impulse-Invariant DTPLL (m=2)**



### 4.6 Summary for Impulse Invariant Method

The following key points are worth repeating:

- Be certain to include **all** unit time delays in your analysis.
- Make every attempt to keep the number of additional unit time delays as small as possible, recognizing that the needed OSR parameter becomes excessive as m>0.

## 5 CTPLL Redesign Using FE Integration Method

If the OSR parameter is very high, any of the redesign methods discussed in this memorandum will work excellently, even the Forward Euler method that will be discussed here. If the OSR parameter is “small” however, great care should be exercised in using this integration method because of its poor stability characteristics. Even before stability factors set in, excessive gain peaking or poor transient response performance may force the adoption of a different integration method.

### 5.1 Closed-Loop Gain Response for FE Method

The first step in computing the closed-loop gain for the FE method is to form the open-loop gain function. The open-loop gain function for the FE method is given by

$$(43) G_{OL}(z) = c \frac{az^{-1} + b}{1 - z^{-1}} \frac{z^{-1}}{1 - z^{-1}}$$

where

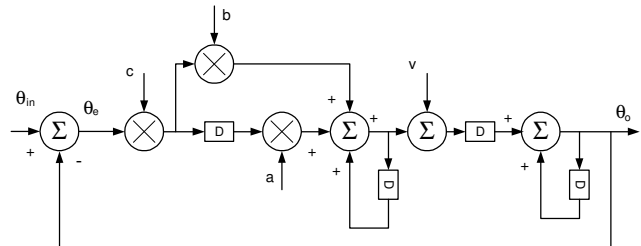
$$(44) \begin{aligned} a &= 1 - b \\ b &= \frac{2\zeta}{\omega_n T} \\ c &= (\omega_n T)^2 \end{aligned}$$

The closed-loop gain that is equivalent to H<sub>1</sub> in equation (28) is given by

$$(45) \frac{\theta_{out}}{\theta_{in}} = \frac{c}{1 + ac} \frac{az^{-2} + bz^{-1}}{z^{-2} + z^{-1} \frac{bc - 2}{1 + ac} + \frac{1}{1 + ac}}$$

and it is shown in block diagram form in Figure 34.

**Figure 34 CTPLL Redesign Using FE Integration Method**



### 5.2 Finite Difference Equation for FE Method

The finite difference equation that describes the transient response for the FE redesign of the CTPLL is given by

$$(46) \begin{aligned} \theta_{out_k} &= ac \theta_{in_{k-2}} + bc \theta_{in_{k-1}} + v_{k-1} - v_{k-2} \\ &- (bc - 2)\theta_{out_{k-1}} - (1 + ac)\theta_{out_{k-2}} \end{aligned}$$

in which  $\theta_{in}$  is the input phase excitation (if present),  $\theta_{out}$  is the output phase at the PLL output, and  $v$  represents an externally applied voltage that can be used to simulate a step-frequency change. The relationship between  $v$  and the applied frequency change is given by  $v = 2\pi F_{step} T$ .

### 5.3 Step-Frequency Response for FE Method

The finite difference equation (46) can be used to easily compute the DTPLL's transient error response to an applied step-change in frequency. Several responses are shown here in the figures that follow for a range of OSR values. OSR values on the order of 30 are required in order to have a good match between the DTPLL'

**Figure 35 DTPLL Transient Response with  $F_s = 5$  kHz (OSR= 3.54)**

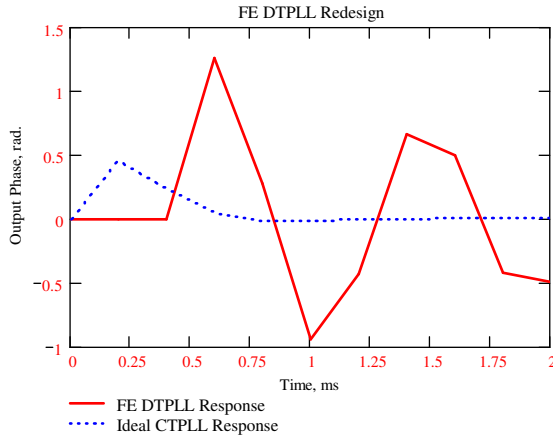


**Figure 36 Closed-Loop Gain Corresponding to Figure 35**

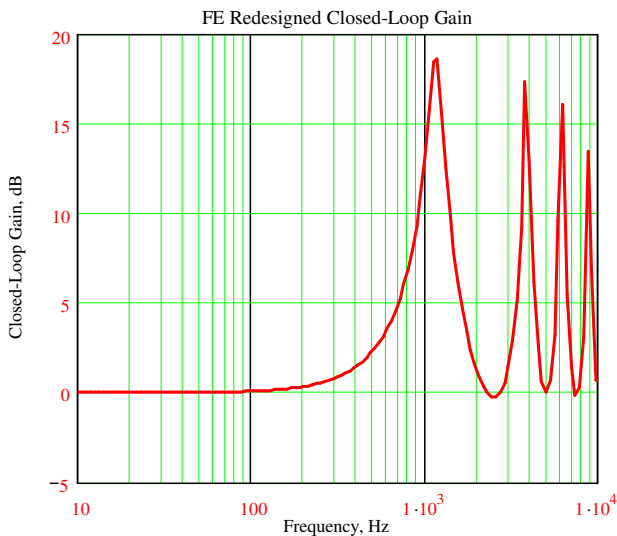


**Figure 37 DTPLL Transient Response with  $F_s = 10$  kHz (OSR= 7.07)**

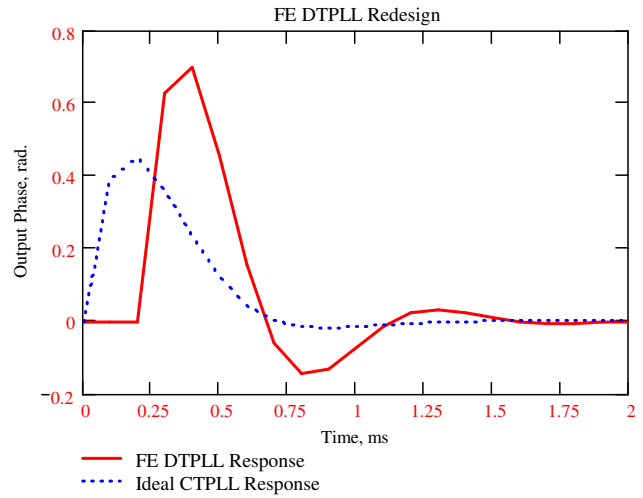


**Figure 38 Closed-Loop Gain Corresponding to Figure 37**

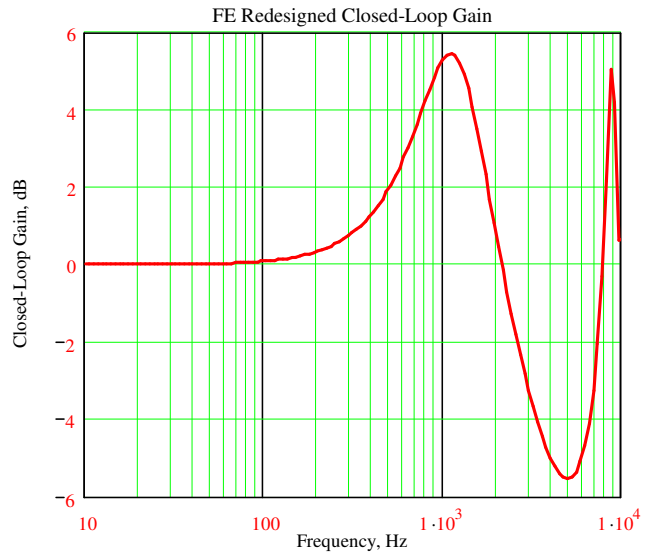


**Figure 39 DTPLL Transient Response with  $F_s=20$  kHz (OSR= 14.14)**

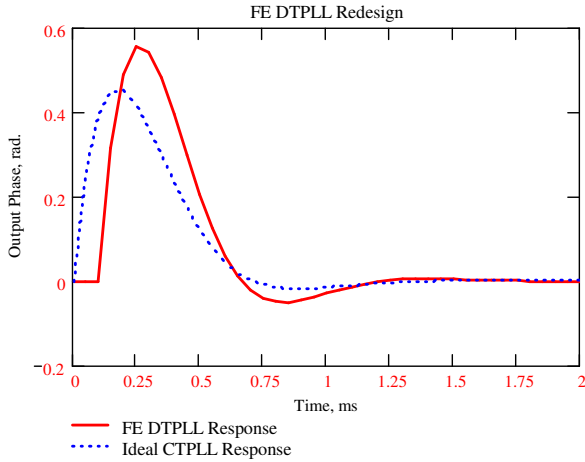


**Figure 42 Closed-Loop Gain Corresponding to Figure 41**



**Figure 40 Closed-Loop Gain Corresponding to Figure 39**



### 5.4 Closed-Loop Gain Peaking

The amount of closed-loop gain peaking is an important measure of loop stability. If the peaking is excessive, more than likely the choice of loop parameters should be adjusted. The closed-loop gain peaking curves for the FE redesigned CTPLL are provided here in Figure 43. As supported by this figure, sampling rates on the order of 40 kHz are required to reduce the influence of sampling rate on gain peaking. For this present example, 40 kHz corresponds to an OSR value of approximately 28.

**Figure 41 DTPLL Transient Response with  $F_s=50$  kHz (OSR= 35.36)**

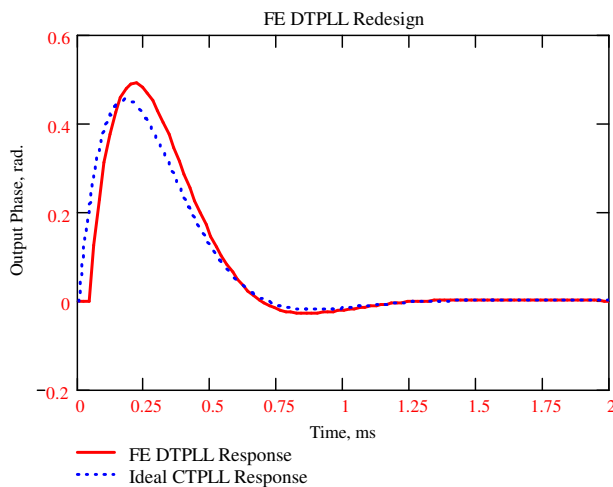
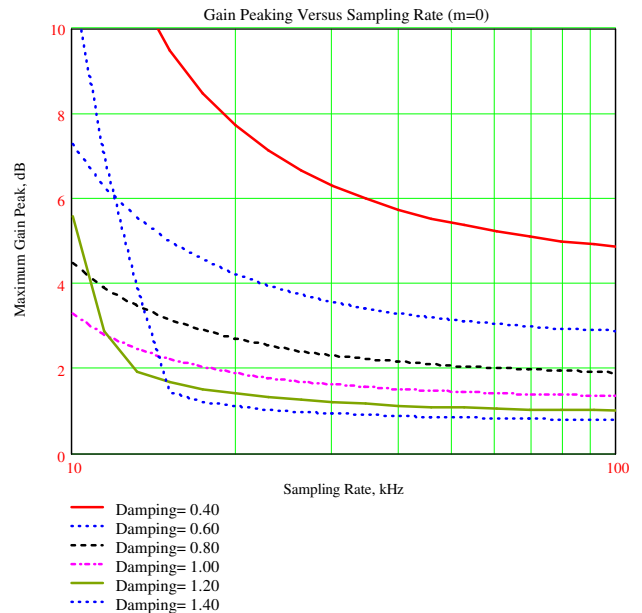


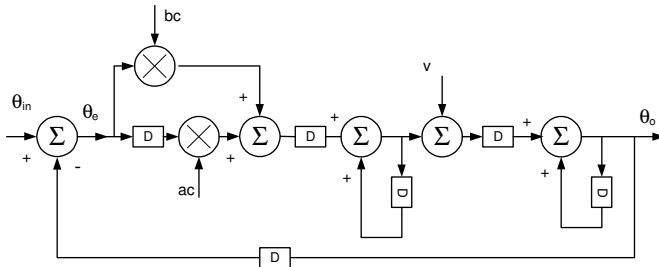
**Figure 43 Closed-Loop Gain Peaking for FE CTPLL Re-Design Versus Damping Factor and Sampling Rate ( $m=0$ )**



### 5.5 FE Method With Additional Time Delay Elements

We have already seen that the inclusion of two additional unit-delays within the impulse-invariant DPLL dramatically affected stability margins for the low sampling rate cases. The same will be true for the FE redesigned CTPLL considered here. A block diagram of the modified DPLL having m=2 additional delays is shown in Figure 44.

**Figure 44 FE Redesigned CTPLL with m=2 Additional Unit-Delay Elements**



The difference equation that describes the transient response for the m=2 case is given by

$$(47) \theta_{out_k} = 2\theta_{out_{k-1}} - \theta_{out_{k-2}} - bc \theta_{out_{k-3}} - ac \theta_{out_{k-4}} + bc \theta_{in_{k-2}} + ac \theta_{in_{k-3}} + v_{k-1} - v_{k-2}$$

Frequency-step transient responses and the corresponding closed-loop gain characteristics are shown for a number of different sampling rates in Figure 45 through Figure 52. The additional delay elements increase the minimum acceptable sampling rate to approximately 25 kHz as compared to about 5 kHz when the delays are absent.

**Figure 45 DTPLL Transient Response with F<sub>s</sub>= 25 kHz (OSR= 17.68, m=2)**

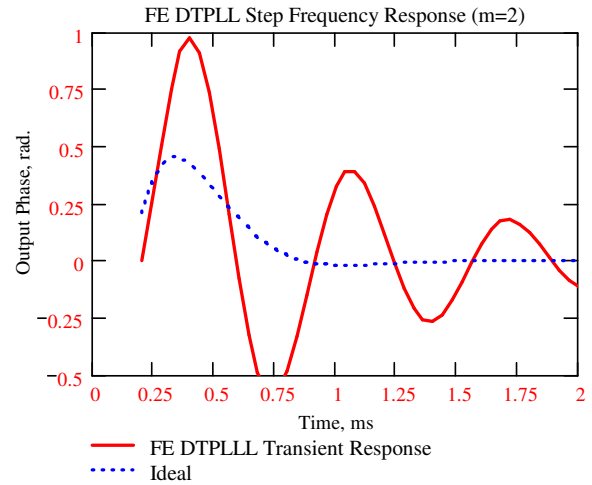


**Figure 46 Closed-Loop Gain Corresponding to Figure 45**

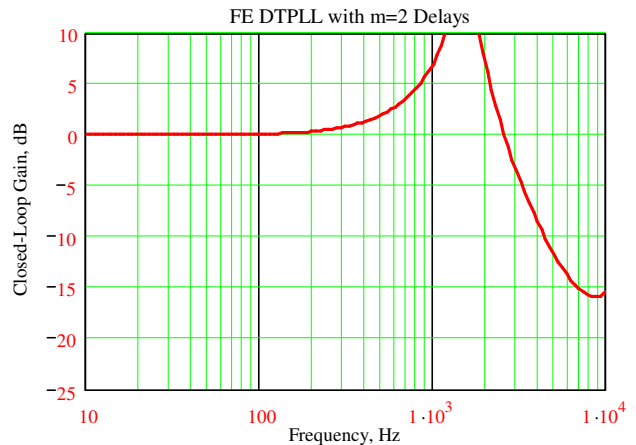


**Figure 47 DTPLL Transient Response with F<sub>s</sub>= 35 kHz (OSR= 24.75, m=2)**

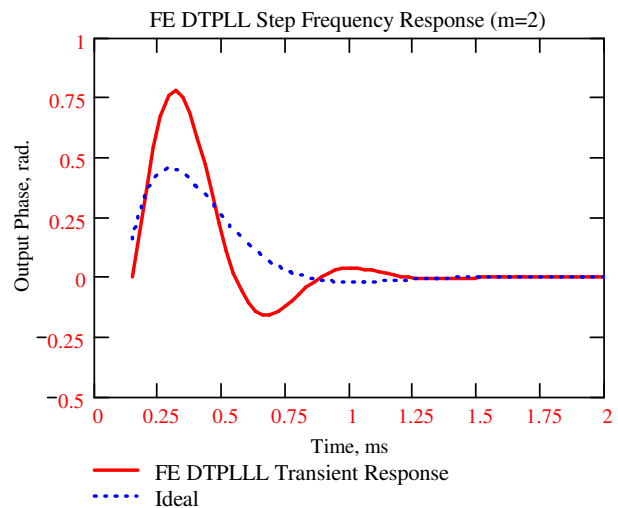


**Figure 48 Closed-Loop Gain Corresponding to Figure 47**

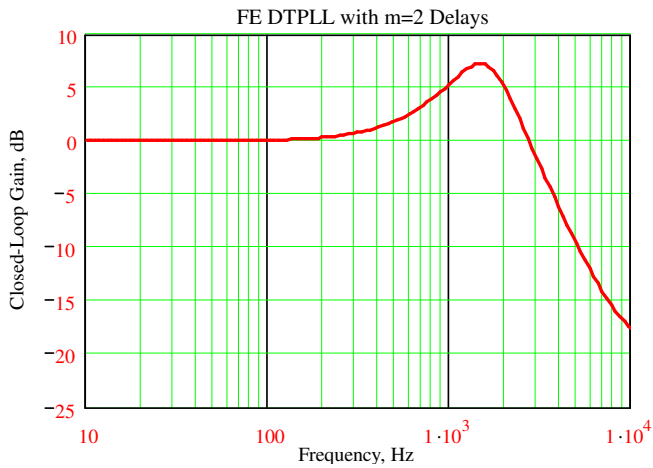


**Figure 51 DTPLL Transient Response with  $F_s = 100$  kHz (OSR= 70.71, m=2)**

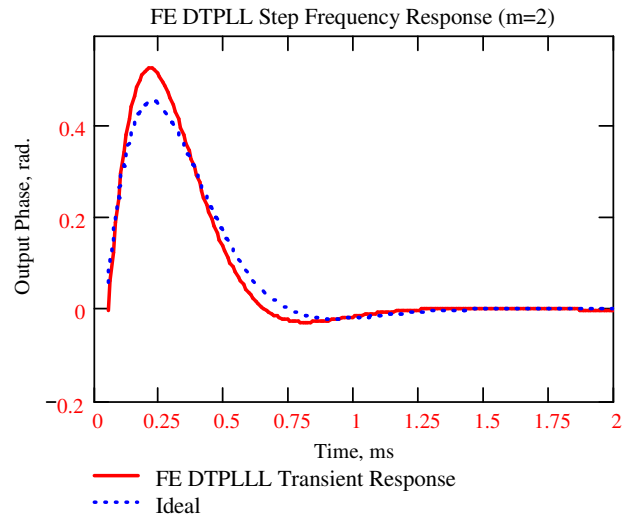


**Figure 49 DTPLL Transient Response with  $F_s = 50$  kHz (OSR= 35.36, m=2)**

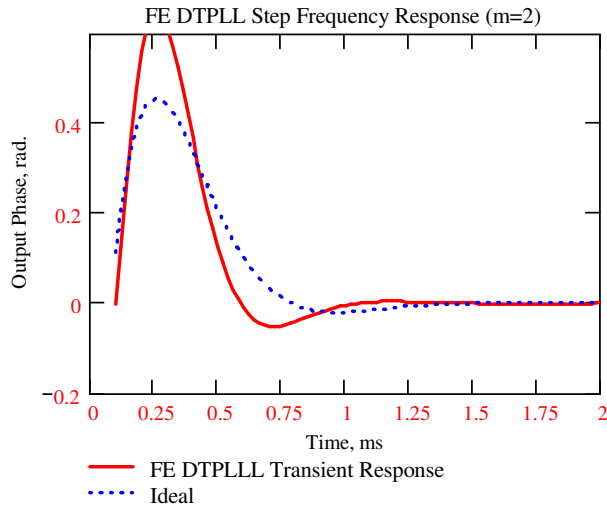


**Figure 52 Closed-Loop Gain Corresponding to Figure 51**

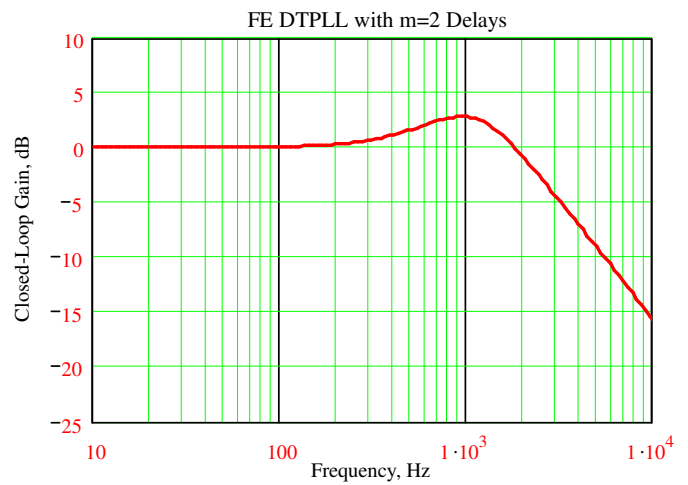
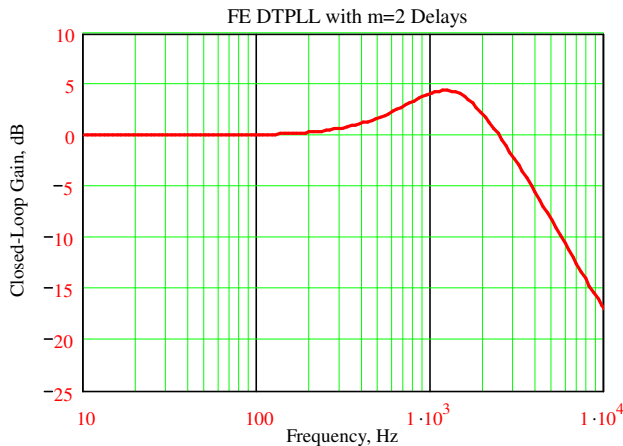


**Figure 50 Closed-Loop Gain Corresponding to Figure 49**



### 5.6 Equivalent Noise Bandwidth

The equivalent closed-loop noise bandwidth can be computed for the FE redesigned CTPLL as done earlier in Section 4.5. The results for the FE redesigned case are provided in Figure 53.

**Figure 53 Equivalent Noise Bandwidth Versus Sampling Rate and Damping Factor for FE Redesigned DTPLL (m=0)**

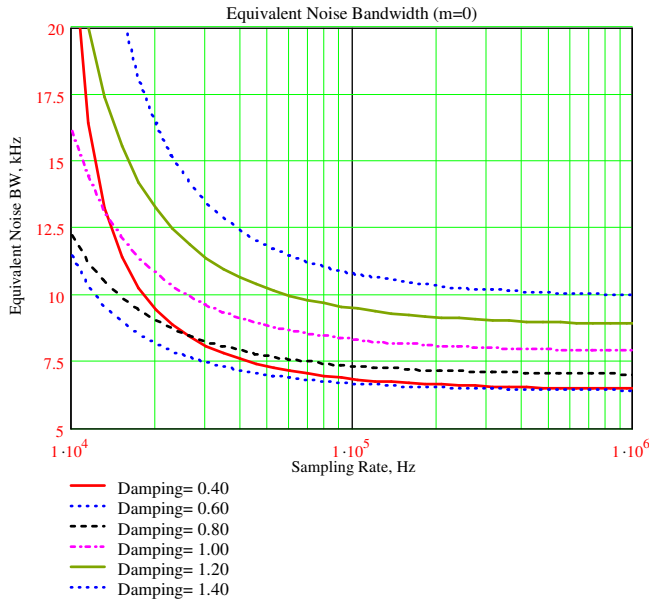
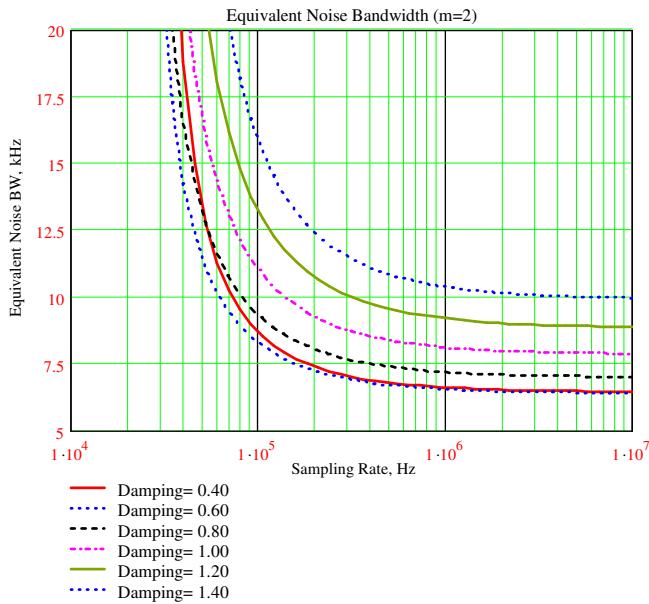


**Figure 54 Equivalent Noise Bandwidth Versus Sampling Rate and Damping Factor for FE Redesigned DTPLL (m=2)**



**5.7 Summary for FE Method**

A comparison of the FE results with the other methods clearly shows that the FE method is less stable as stated earlier. Although the FE method can be made to work equally well given a sufficiently high OSR value, other methods that are discussed in this

memorandum are superior and should be adopted whenever possible.

**6 CTPLL Redesign Using BE Integration Method**

The Backward Euler (BE) method is the first implicit integration method that will be considered. Although its region of stability is still less than that delivered by the trapezoidal method (i.e., bilinear transform method), it can be adopted with confidence as circumstances warrant.

**6.1 Finite Difference Equation for BE Method**

The first step in computing the closed-loop gain for the BE method is to form the open-loop gain function. The open-loop gain function for the FE method is given by

$$(48) G_{OL}(z) = c \frac{az^{-1} + b}{1 - z^{-1}} \frac{1}{1 - z^{-1}}$$

where

$$a = -\frac{2\zeta}{\omega_n T}$$

$$(49) b = 1 - a$$

$$c = (\omega_n T)^2$$

The closed-loop gain that is equivalent to  $H_1$  in equation (28) is given by

$$(50) \frac{\theta_{out}}{\theta_{in}} = \frac{acz^{-1} + bc}{z^{-2} + z^{-1}(ac - 2) + (1 + bc)}$$

and it is shown in block diagram form in Figure 55.

Figure 55 CTPLL Redesign Using BE Integration Method

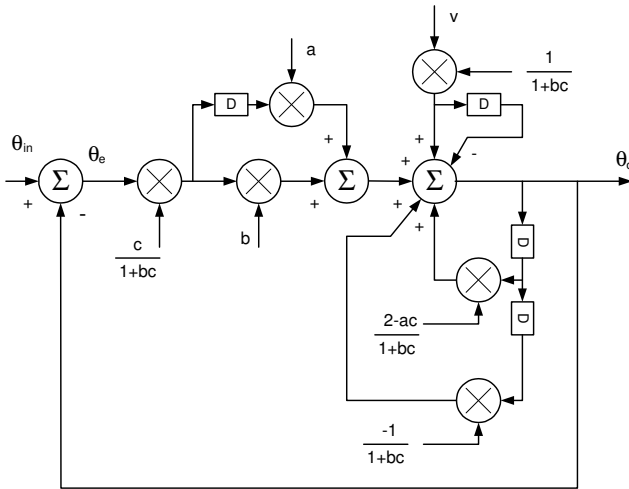


Figure 57 Closed-Loop Gain Corresponding to Figure 56

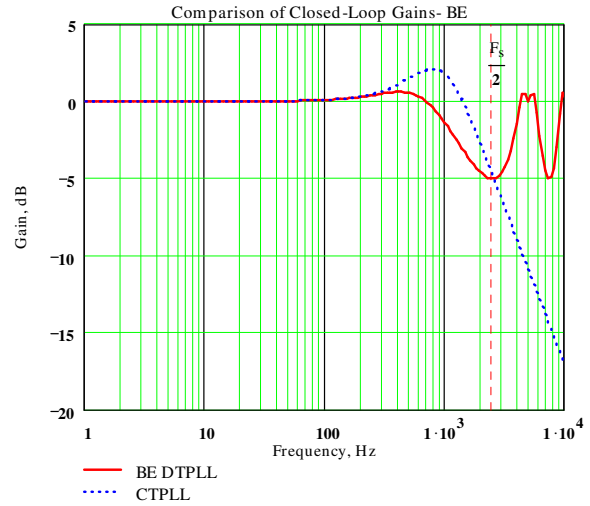
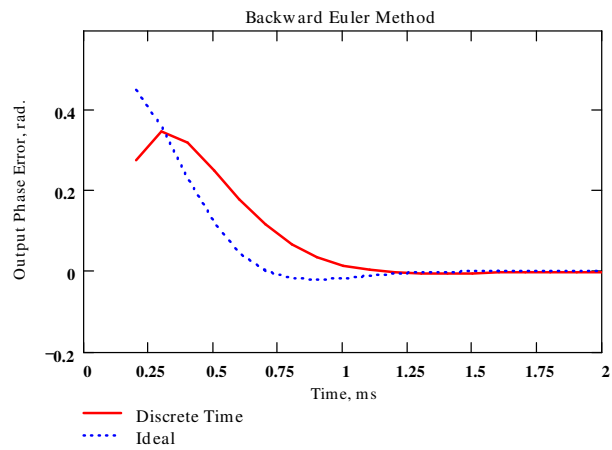


Figure 58 Transient Response with F<sub>s</sub>= 10 kHz (OSR= 7.07)



## 6.2 Step-Frequency Response for BE Method

The finite difference equation that describes the DPLL's transient response to input frequency and phase modulation is given by

$$(51) \theta_{out_k} = (1 + bc)^{-1} \left\{ ac \theta_{in_{k-1}} + bc \theta_{in_k} + v_k - v_{k-1} \right. \\ \left. + \theta_{out_{k-1}} (2 - ac) - \theta_{out_{k-2}} \right\}$$

Several representative step-frequency transient responses are shown as a function of sampling rate in the figures that follow.

Figure 56 DTPLL Transient Response with F<sub>s</sub>= 5 kHz (OSR= 3.536)

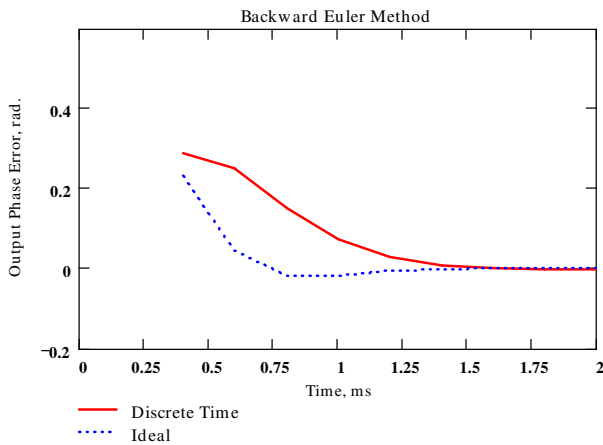
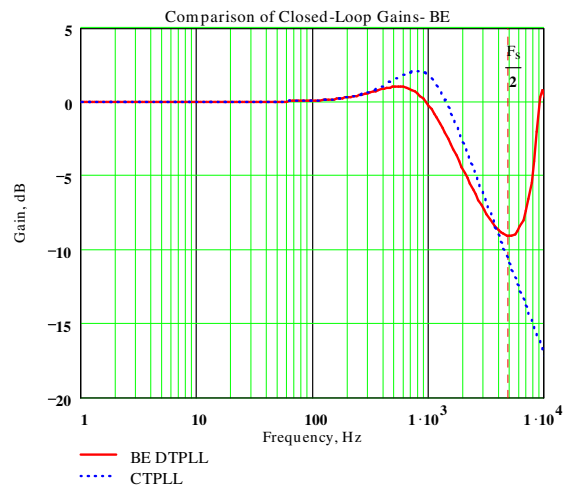
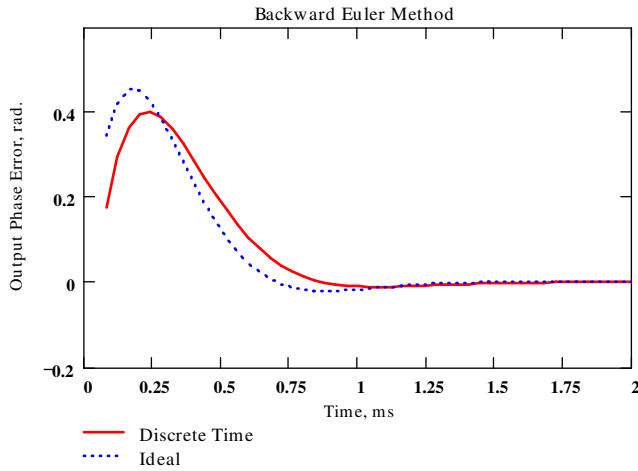


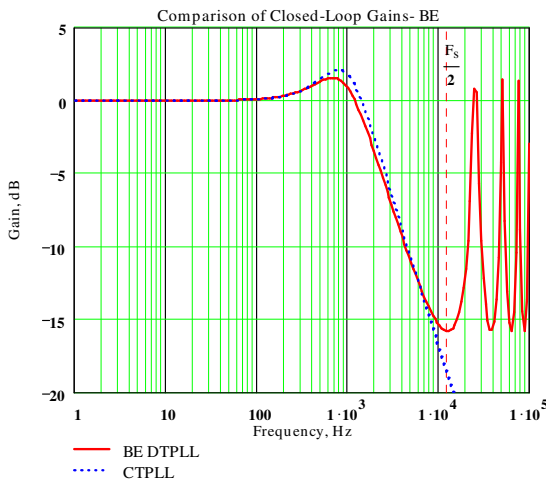
Figure 59 Closed-Loop Gain Corresponding to Figure 58



**Figure 60 Transient Response with  $F_s= 25$  kHz (OSR= 17.68)**



**Figure 61 Closed-Loop Gain Corresponding to Figure 60**



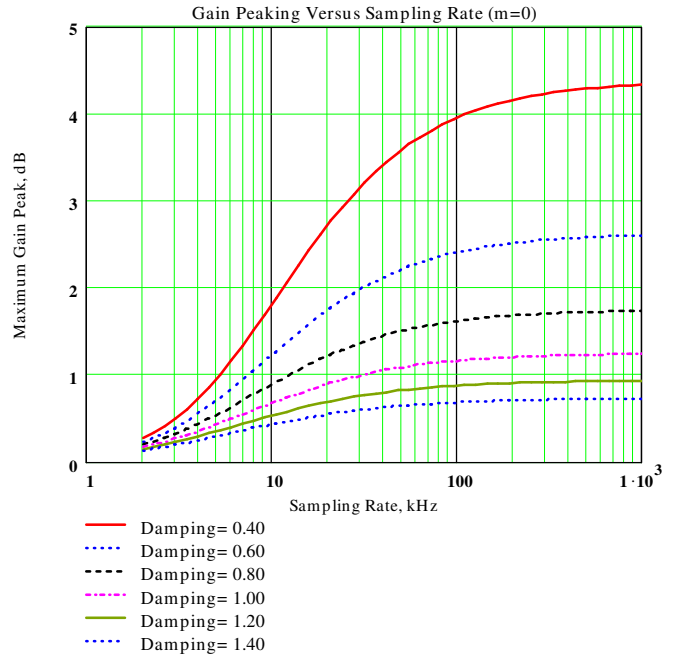
**6.3 Closed-Loop Gain Peaking for BE Method**

The amount of closed-loop gain peaking is an important measure of loop stability. If the peaking is excessive, more than likely the choice of loop parameters should be adjusted. The closed-loop gain peaking curves for the BE redesigned CTPLL are provided here in Figure 62. As supported by this figure, sampling rates on the order of 40 kHz are required to reduce the influence of sampling rate on gain peaking. For this present example, 40 kHz corresponds to an OSR value of approximately 28.

These gain-peaking curves are dramatically different than the curves provided in Figure 31 and Figure 43 for the impulse-invariant and FE methods. Low sampling rates in the FE methods lead to lower closed-loop bandwidths whereas they lead to instability

with the impulse-invariant and FE methods. This improvement in stability is due to the implicit nature of the BE algorithm as compared to these other two methods.

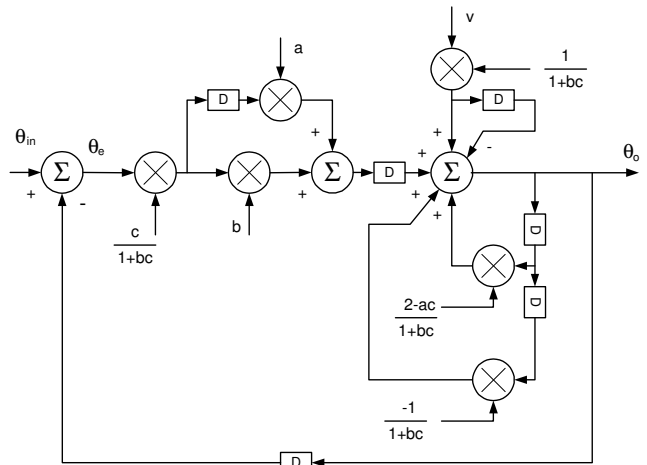
**Figure 62 Closed-Loop Gain Peaking for BE CTPLL Re-Design Versus Damping Factor and Sampling Rate ( $m=0$ )**



**6.4 BE Method With Additional Time Delay Elements**

Two additional unit-delays have been inserted in Figure 63 in order to ease implementation.

**Figure 63 CTPLL Redesign Using BE Integration Method Including Additional Delays ( $m=2$ )**



The finite difference equation that describes the transient response for the BE case with  $m=2$  is given by

$$(52) \quad \theta_{out_k} = ac \theta_{in_{k-2}} + bc \theta_{out_{k-3}} + v_k - v_{k-1} + 2\theta_{out_{k-1}} - (1+bc)\theta_{out_{k-2}} - ac \theta_{out_{k-3}}$$

This result can be used to compute the resulting step-frequency transient responses as shown in the following figures.

**Figure 64 Transient Response with  $F_s=25$  kHz (OSR= 17.68,  $m=2$ )**

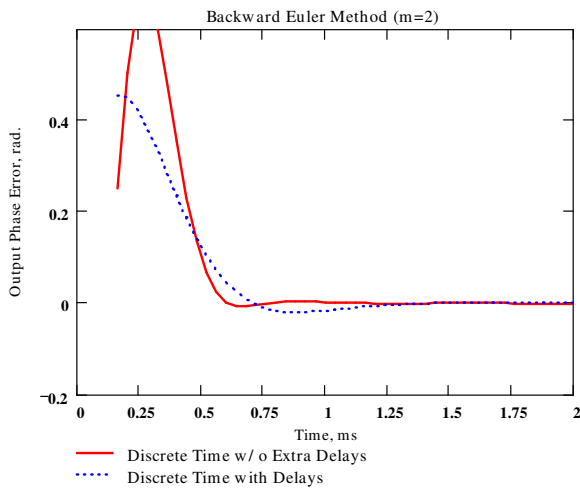


**Figure 65 Closed-Loop Gain Corresponding to Figure 64**

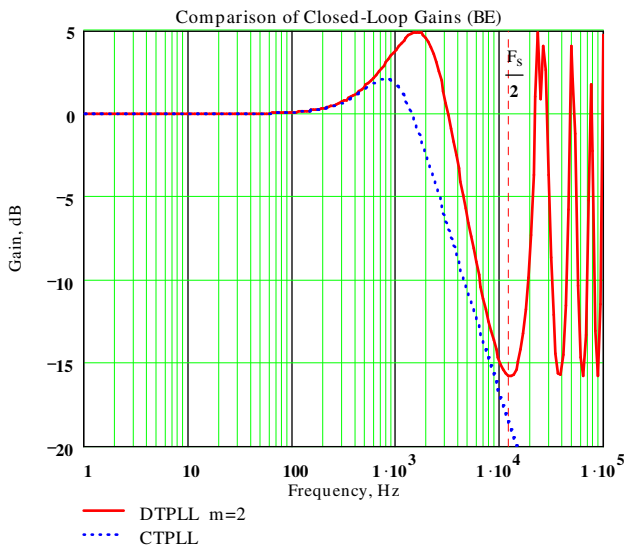


**Figure 66 Transient Response with  $F_s=50$  kHz (OSR= 35.36,  $m=2$ )**

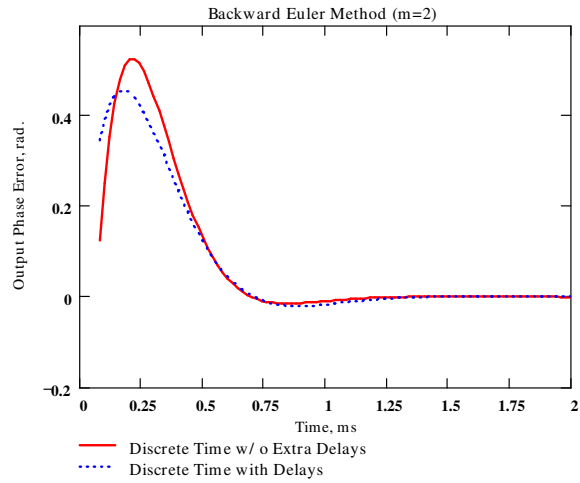


**Figure 67 Closed-Loop Gain Corresponding to Figure 66**

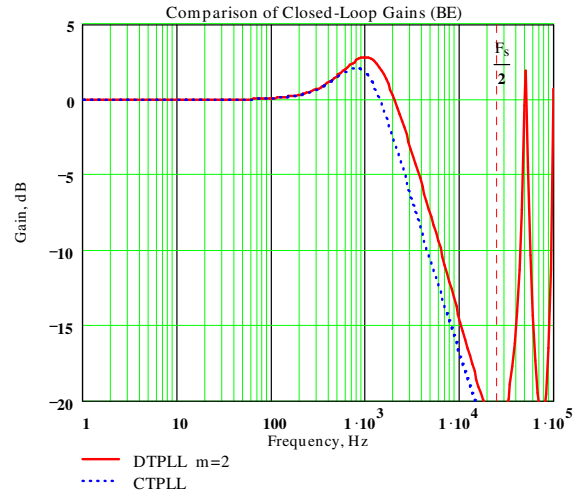


**Figure 68 Transient Response with  $F_s=100$  kHz (OSR= 70.71,  $m=2$ )**

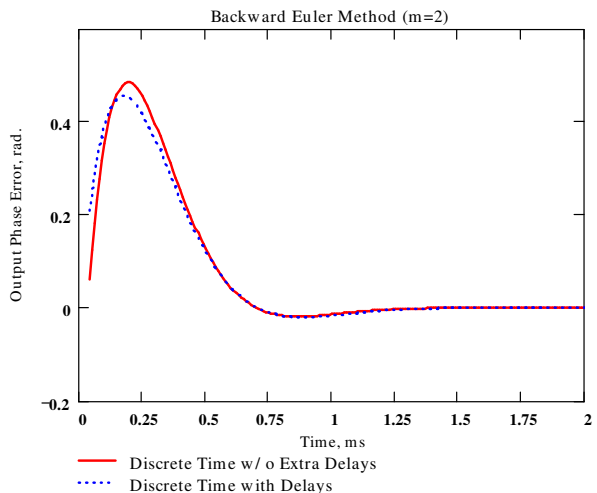


Figure 69 Closed-Loop Gain Corresponding to Figure 68

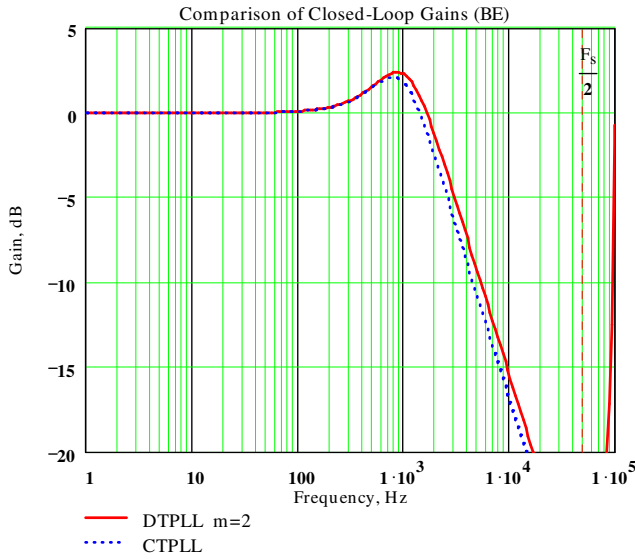
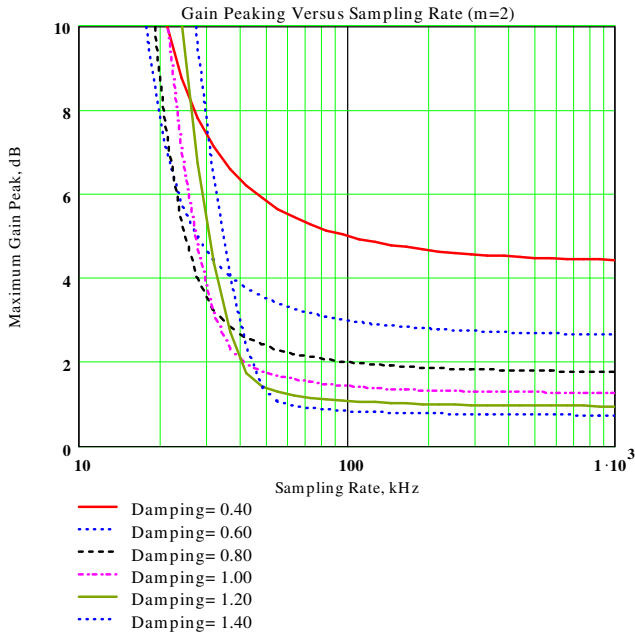


Figure 70 Gain Peaking for BE Method With m=2 Additional Delays Present



### 6.5 Equivalent Noise Bandwidth for BE Method

The equivalent noise bandwidth for the BE DTPLL are shown for the m=0 and m=2 cases in Figure 71 and Figure 72 respectively.

Figure 71 Equivalent Noise Bandwidth for BE Method (m=0)

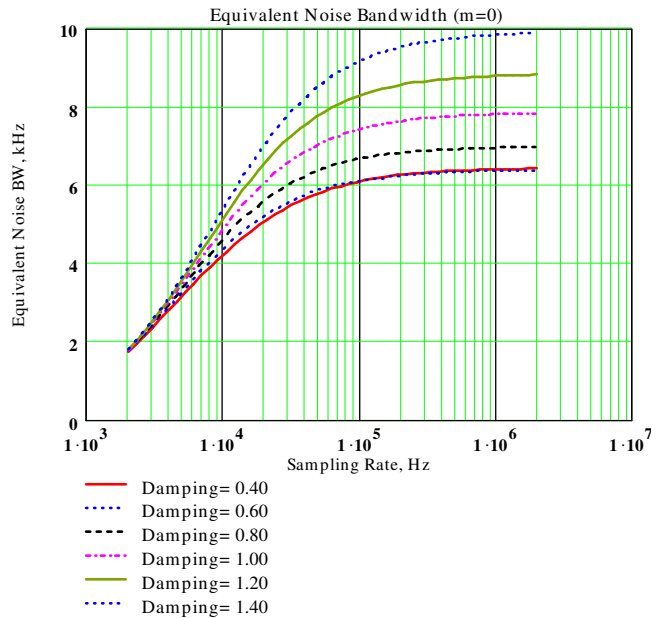
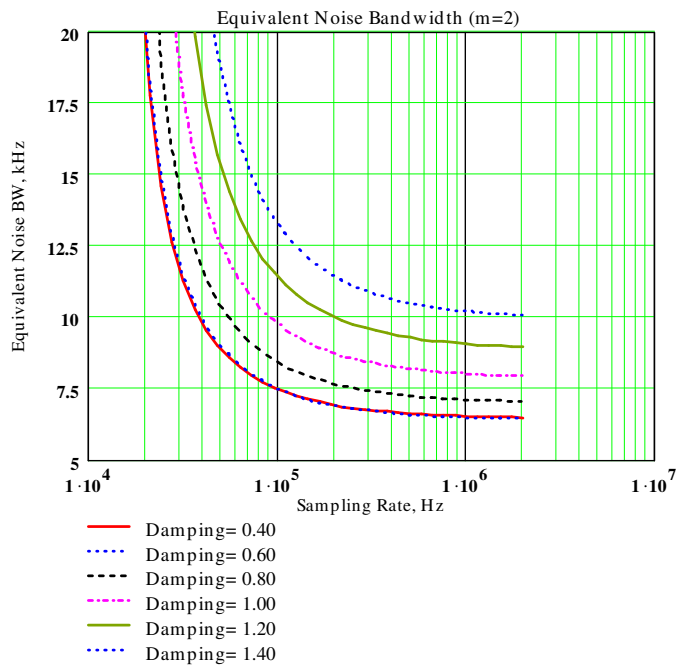


Figure 72 Equivalent Noise Bandwidth for BE Method (m=2)



## 6.6 Summary for BE Method

The BE method clearly exhibits substantially better stability than the FE method because it is based upon an implicit integration formula as discussed earlier. The block diagram for this method shown in Figure 55 is nevertheless fairly complex for a second-order system. As shown in the next section, the bilinear transform method exhibits a more simplified block diagram (see Figure 73) even though it too is an implicit second-order system formulation.

## 7 CTPLL Redesign Using Bilinear Transform Method

The bilinear transform method (BT), also known as the trapezoidal method, is probably the most prevalent redesign method that is used. It has excellent stability characteristics as discussed earlier in Section 2.3. In most cases, this method is the **preferred method** to use and for that reason, we will spend additional time on this important re-design approach.

### 7.1 Finite Difference Equation for BT Method

The open-loop gain characteristic for the BT method is given by

$$(53) G_{OL}(z) = c \frac{az^{-1} + b}{1 - z^{-1}} \frac{1 + z^{-1}}{1 - z^{-1}}$$

where

$$a = 1 - \frac{4\zeta}{\omega_n T}$$

$$(54) b = 1 + \frac{4\zeta}{\omega_n T}$$

$$c = \left( \frac{\omega_n T}{2} \right)^2$$

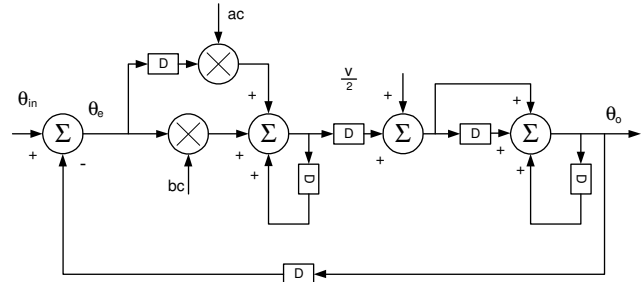
Sometimes, designers predestort the natural frequency  $\omega_n$  to compensate for the frequency warping characteristics of the bilinear transform. This can be done for any pole or zero location in the Laplace domain  $p_o$  and converting it to the appropriate pole or zero in the z-domain as

$$(55) z_p = \left( 1 + \frac{p_o T_s}{2} \right) \left( 1 - \frac{p_o T_s}{2} \right)^{-1}$$

However, no frequency pre-distortion is used in the discussions that follow.

The block diagram for the BT DTPLL is provided in Figure 73.

**Figure 73 Block Diagram for BT DTPLL Redesign Method**



### 7.2 Stability of BT-Based DTPLL

The stability of the BT method when used to simulate the Type-2 CTPLL is exceptional. That is not to say that the DPLL exactly mimics the CTPLL for low OSR values, but rather that it is extremely stable even for low OSR values.

The phase margin can be found by first computing the frequency at which the open-loop gain is unity. After a fair amount of algebra, it can be shown that the unity-gain frequency is given by

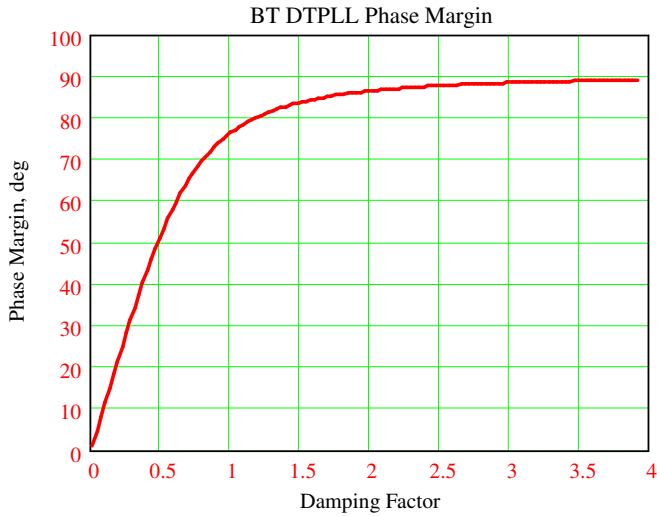
$$(56) \omega_{unity} = \frac{1}{T} \cos^{-1} \left[ \frac{1 + \left( \frac{\omega_n T}{2} \right)^4 - 2 \left( \frac{\omega_n T}{2} \right)^2 \sqrt{1 + 4\zeta^4}}{1 + (\zeta \omega_n T)^2 - \left( \frac{\omega_n T}{2} \right)^4} \right]$$

The phase margin can be computed using this result in equation (53) to compute the open-loop phase. The end result is that the phase margin is given very accurately (within about 0.2 degrees for  $0 < \zeta < 4$ ) by the approximation

$$(57) PM(\zeta) = \tan^{-1} \left( \frac{\alpha_1 \zeta + \alpha_2 \zeta^2 + \alpha_3 \zeta^4}{1 + \alpha_4 \zeta^2} \right)$$

in which  $\alpha_1 = 1.80746$ ,  $\alpha_2 = 2.8674$ ,  $\alpha_3 = 22.26795$ ,  $\alpha_4 = 5.54267$ . The phase margin versus damping factor is shown here in Figure 74. The analysis reveals that the phase margin for this specific case is independent of the sampling rate and natural frequency selection for all practical choices (i.e.,  $OSR > 2$ ) which is obviously a very desirable result.

Figure 74 Phase Margin for BT DTPLL (m=0)



The gain margin is undefined for the DTPLL case because the phase of the open loop gain does not become  $\pm 180$  degrees except for frequencies greater than  $F_s/2$ .

### 7.3 Step-Frequency Response for BT Method

The difference equation that describes the transient response for the BT DTPLL is given by

$$(58) \theta_{o_k} = \frac{1}{1+bc} \left[ \frac{bc \theta_{i_k} + (ac+bc)\theta_{i_{k-1}} + ac \theta_{i_{k-2}} + \frac{v_k - v_{k-2}}{2}}{(2-ac-bc)\theta_{o_{k-1}} - (1+ac)\theta_{o_{k-2}}} \right]$$

in which a, b and c are defined by (54). A number of example transient responses are shown in Figure 75 through Figure 83. As suggested by earlier comments regarding the BT method, the transient responses are very well behaved even for fairly small values of the OSR parameter.

Figure 75 Transient Response for BT DPLL with  $F_s = 8$  kHz (OSR= 5.66)

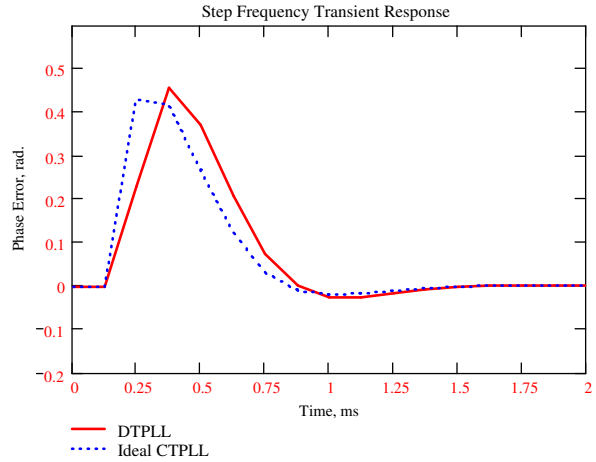
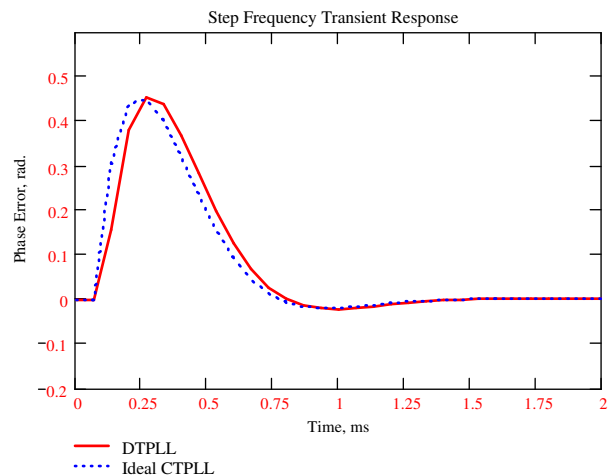


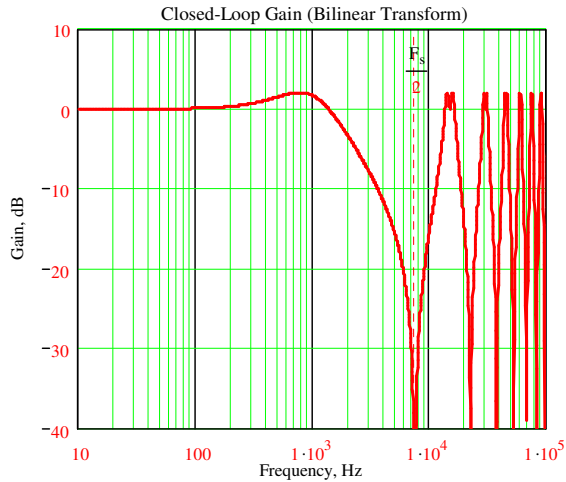
Figure 76 Closed-Loop Gain Corresponding to Figure 75



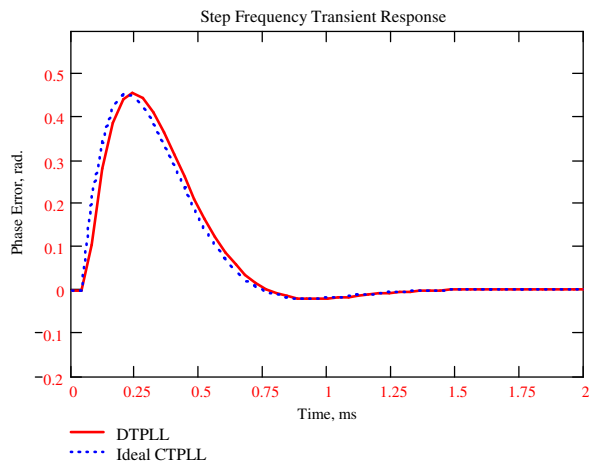
Figure 77 78 Transient Response for BT DPLL with  $F_s = 15$  kHz (OSR= 10.61)



**Figure 79 Closed-Loop Gain Corresponding to Figure 77**



**Figure 80 Transient Response for BT DPLL with  $F_s = 25$  kHz (OSR= 17.68)**



### 7.4 BT Method With Additional Time Delay Elements

Two additional delay elements have been added to the DTPLL in Figure 84 in order to ease implementation. Gain-peaking and equivalent noise bandwidth for this case are addressed separately in Sections 7.5 and 7.6 respectively.

The finite difference equation that describes the transient response of this modified DPLL is given by

$$\theta o_k = bc \theta i_k + c(a+b)\theta i_{k-1} + ac \theta i_{k-2} +$$

$$(59) \quad \frac{v_k - v_{k-2}}{2} +$$

$$(2-bc)\theta o_{k-1} - [1+c(a+b)]\theta o_{k-1} - ac \theta o_{k-3}$$

Several step-frequency transient responses are shown for the m=2 case in Figure 81 through Figure 91.

**Figure 81 Closed-Loop Gain Corresponding to Figure 80**

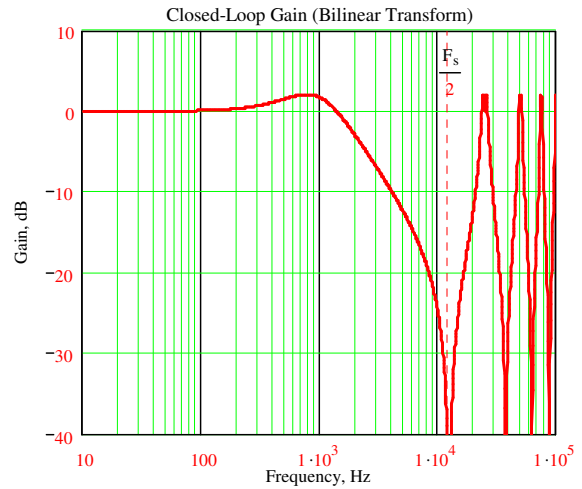


**Figure 82 Transient Response for BT DPLL with  $F_s = 50$  kHz (OSR= 35.36)**

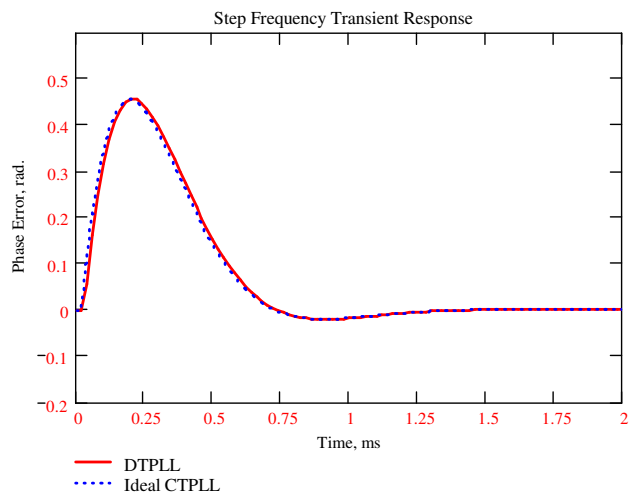




**Figure 88 Closed-Loop Gain Corresponding to Figure 87**

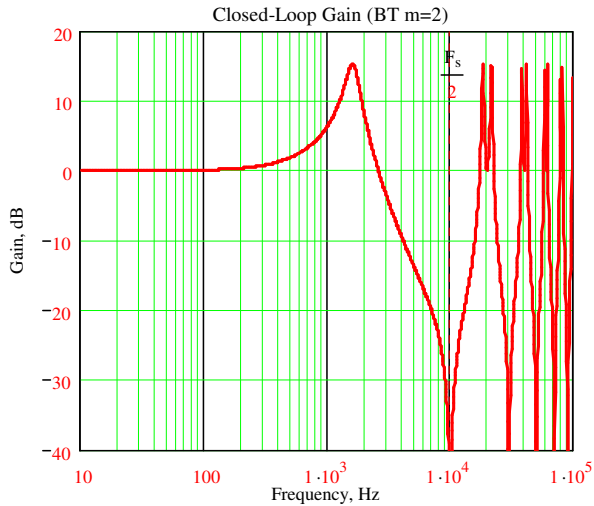


**Figure 91 Transient Response for BT DPLL with  $F_s = 100$  kHz (OSR= 70.71, m=2)**

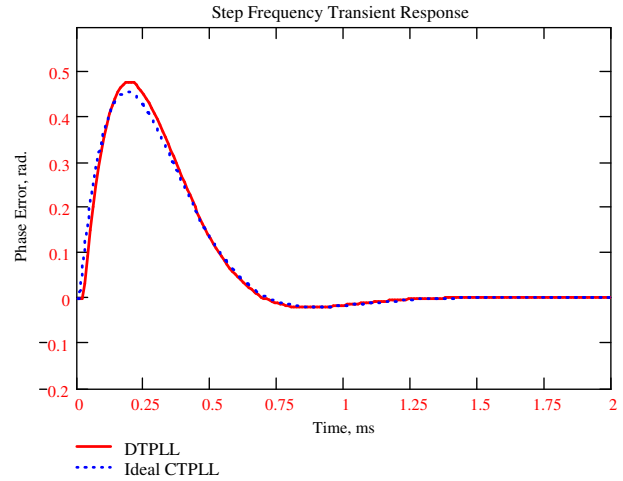


**Figure 89 Transient Response for BT DPLL with  $F_s = 50$  kHz (OSR= 35.36, m=2)**

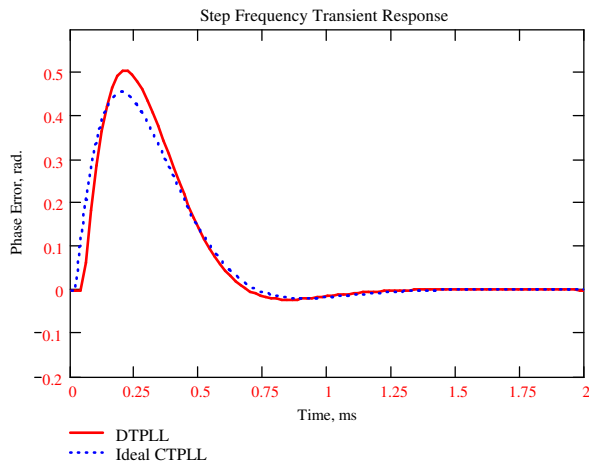


**Figure 92 Closed-Loop Gain Corresponding to Figure 91**

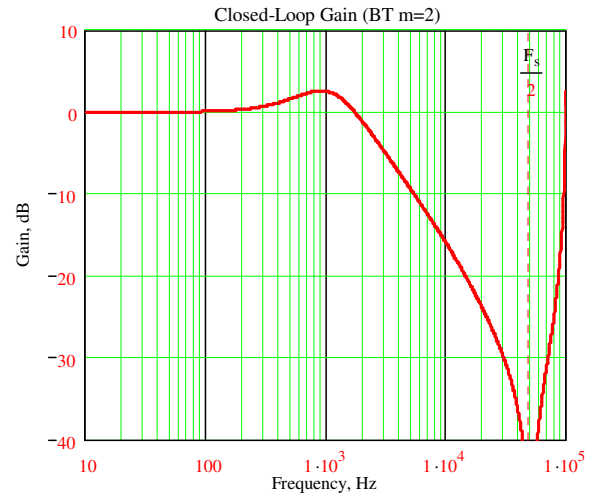
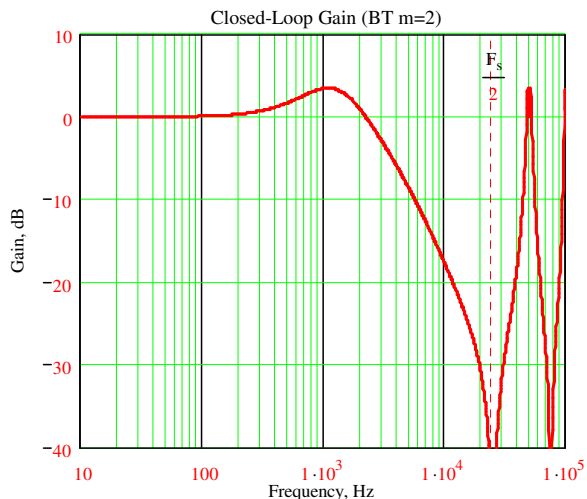


**Figure 90 Closed-Loop Gain Corresponding to Figure 89**



### 7.5 Closed-Loop Gain Peaking for BT Method

As done for the previous cases, it is a straight forward to compute the maximum gain peaking that occurs versus damping factor and sampling rate. In all cases, a natural frequency of 1 kHz is again assumed. The results for the m=0 and m=2 cases are shown in Figure 93 and Figure 94 respectively. Both of these results are have very attractive performance characteristics.

### 7.6 Equivalent Noise Bandwidth for BT Method

The equivalent noise bandwidth behavior versus damping factor and sampling rate for the BT m=0 and

$m=2$  cases are shown in Figure 95 and Figure 96. Large equivalent noise bandwidths are indicative of excessive gain peaking of course.

**Figure 93 Gain Peaking for BT DTPLL With No Additional Internal Delays ( $m=0$ )**

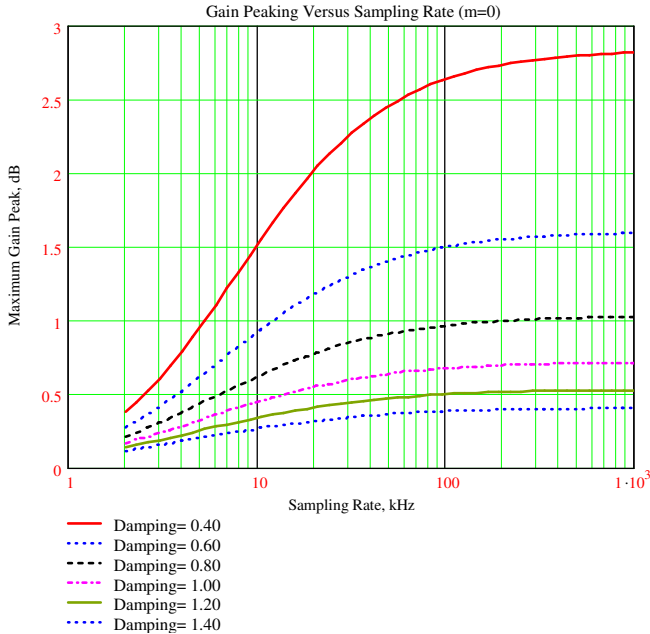


**Figure 94 Gain Peaking for BT DTPLL With Additional Internal Delays ( $m=2$ )**

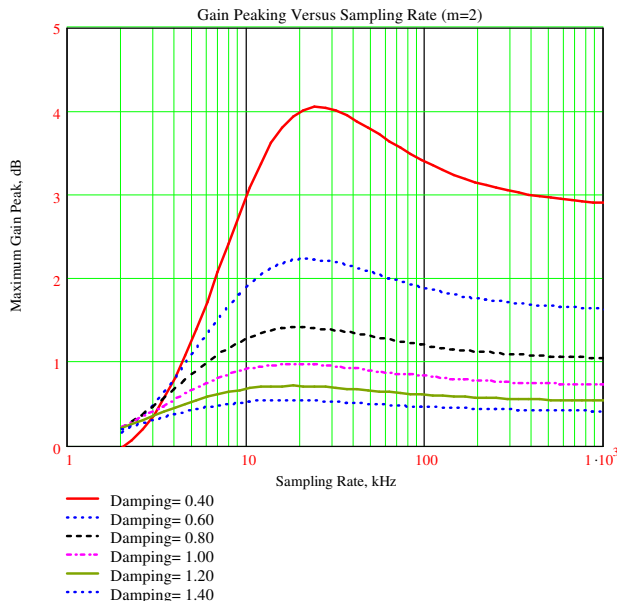


**Figure 95 Equivalent Noise Bandwidth for BT DTPLL With No Additional Internal Delays ( $m=0$ )**

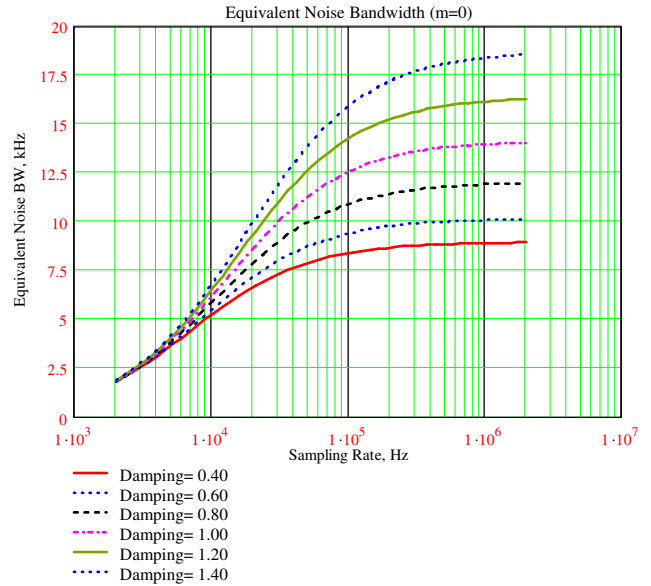
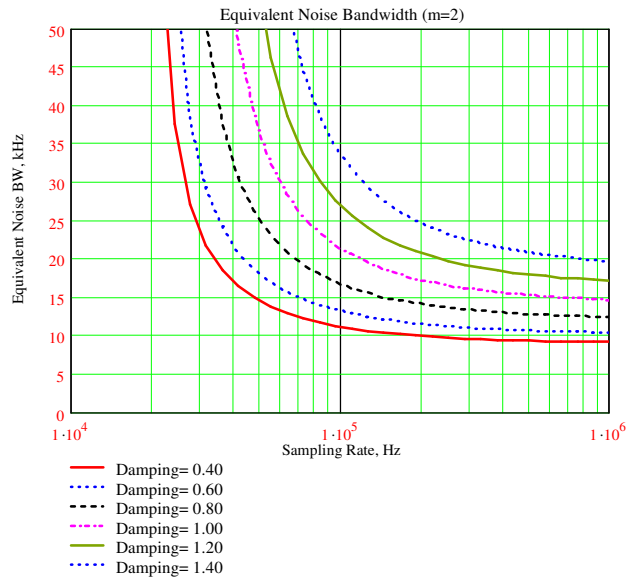


**Figure 96 Equivalent Noise Bandwidth for BT DTPLL With Additional Internal Delays ( $m=2$ )**



### 7.7 Summary for BT Method

The BT method is to be preferred for redesigning CTPLL's in most cases. It exhibits very desirable stability characteristics and is also straight forward to implement.

## 8 CTPLL Redesign Using 2<sup>nd</sup>-Order Gear Method

The 2<sup>nd</sup> Order Gear Method involves substantially more complexity in its implementation. Although this integration formula has desirable attributes in the context of stiff differential equations, the added complexity in the implementation would normally require that additional unit-delay elements be inserted thereby detracting from its suitability. The open-loop gain is given by the expression

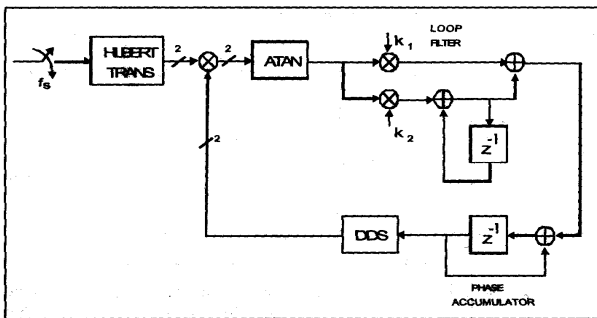
$$(60) G_{ol}(z) = \left( \frac{2\omega_n T}{3} \right)^2 \frac{1 + \frac{3\zeta}{\omega_n T} \left( 1 - \frac{4}{3}z^{-1} + \frac{1}{3}z^{-2} \right)}{\frac{3}{2T} \left( 1 - \frac{4}{3}z^{-1} + \frac{1}{3}z^{-2} \right)^2}$$

which obviously bears considerable complexity. Consequently, this method will not be pursued further at this time.

## 9 Other PLL Redesign Literature

A DSP-based PLL that utilizes an arctangent phase detector and direct digital synthesizer (DDS) quadrature oscillator are discussed in [5]. A block diagram of the PLL is provided here in

**Figure 97 DSP Based PLL with ATAN Phase Detector and DDS Quadrature Oscillator**



The z-transform for the DPLL is given by

$$(61) \frac{\theta_o(z)}{\theta_i(z)} = \frac{(k_1 + k_2) \left( z - \frac{k_2}{k_1 + k_2} \right)}{z^2 - 2 \left( 1 - \frac{k_1 + k_2}{2} \right) z + (1 - k_1)}$$

The gain terms  $k_1$  and  $k_2$  can be expressed in terms of the CTPLL parameters  $\omega_n$  and  $\zeta$  as

$$(62) \begin{aligned} k_1 &= \frac{4\phi^2}{1 + 2\zeta\phi + \phi^2} \approx \frac{4\phi^2}{1 + 2\zeta\phi} \\ k_2 &= \frac{4\zeta\phi}{1 + 2\zeta\phi + \phi^2} \approx \frac{4\zeta\phi}{1 + 2\zeta\phi} \end{aligned}$$

in which

$$(63) \phi = \pi \frac{\omega_n}{\omega_s}$$

The design parameters ( $k_1$  and  $k_2$ ) are derived from the analog PLL loop by using the bilinear z-transform and then comparing the denominator expressions (characteristic functions) of the two transfer functions.

Many other PLL re-design methodologies may be employed from ad-hoc methods to fairly sophisticated Kalman filter based methods. A reasonably broad overview of many of these different perspectives is provided in [1].

## 10 Conclusions and Recommendations

As we have seen, stability in the PLL re-design sense comes in two distinctly different forms: (1) stability of the underlying numerical integration formula, and (2) stability of the DPLL design (assuming ideal numerical integration). Both perspectives must be considered.

Different metrics can be adopted to guide the re-design methodology that is followed. These included concepts such as impulse invariance, equivalent noise bandwidth, etc.

It is very easy to have additional delays within the DPLL that are overlooked in the analysis. The impact is not severe if the over-sampling rate is extremely large, but stability and performance can suffer greatly if this is not the case.

The trapezoidal integration formula which is equivalent to the bilinear transform is very attractive based upon both its simplicity and region of stability. In most cases, this method should be preferred over the other integration methods that were presented.

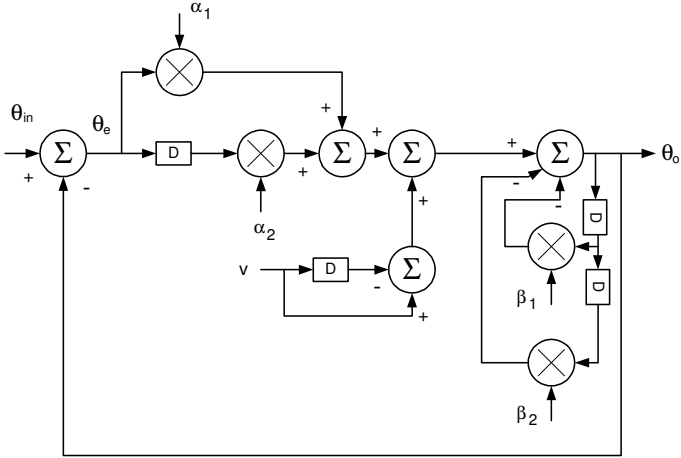
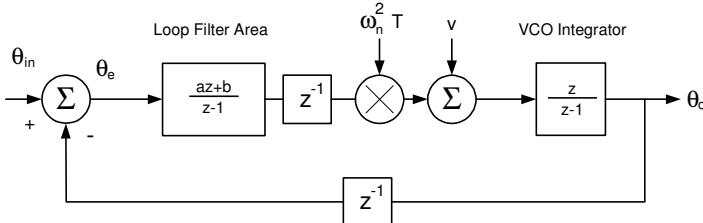
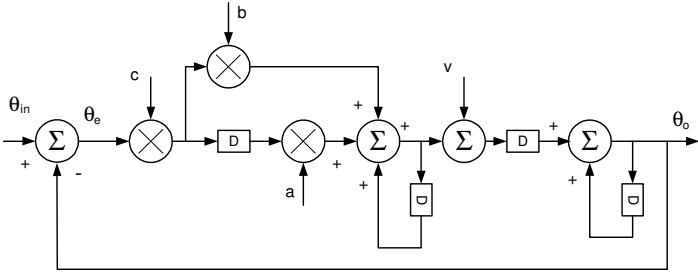
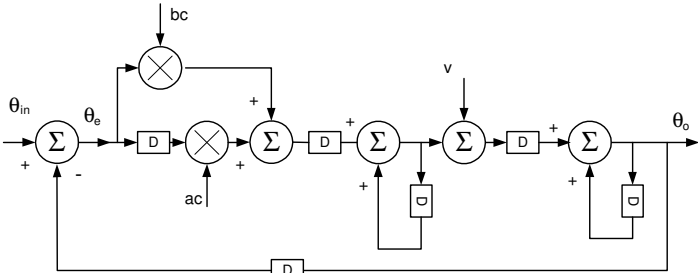
## 11 References

1. Crawford, J.A., "Phase-Locked Loops- A Broad Perspective", CommsDesign 5 May 2004, <http://www.commsdesign.com/showArticle.jhtml?articleID=19502344>
2. \_\_\_\_\_, *Frequency Synthesizer Design Handbook*, Artech House, 1994
3. Chua, L.O., Lin, P., *Computer-Aided Analysis of Electronic Circuits: Algorithms and Computational Techniques*, Prentice-Hall, 1975
4. Dorf, R.C., *Modern Control Systems*, 2<sup>nd</sup> Ed., Addison-Wesley Publishing Co., 1974
5. Harris, F., "A Tutorial: Phase Locked Loops in DSP Based Modems",

**Contact Information:**

E-mail: [xo@am1.us](mailto:xo@am1.us)  
Website: [www.am1.us](http://www.am1.us)

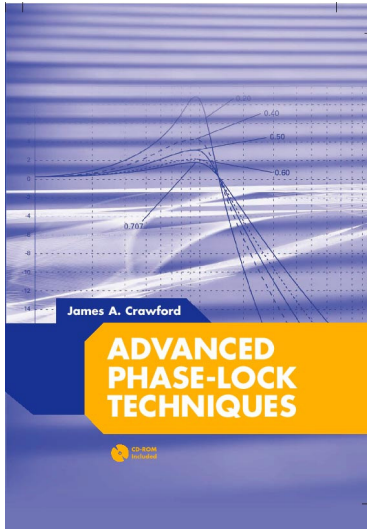
## 12 Summary of CTPLL Redesign Formula

Name	Block Diagram	Coefficients	Recommended OSR Range
Impulse Invar. m=0		$\alpha_1 = ac$ $\alpha_2 = bc$ $\beta_1 = bc - 2$ $\beta_2 = 1$ $a = \frac{2\zeta}{\omega_n}$ $b = T - \frac{2\zeta}{\omega_n}$ $c = \omega_n^2 T$	$\geq 7$ for $\zeta = 0.707$
Impulse Invar. m=2		<p>Same as Impulse Invariance</p>	$\geq 50$ for $\zeta = 0.707$
FE m=0		$a = 1 - b$ $b = \frac{2\zeta}{\omega_n T}$ $c = (\omega_n T)^2$	<p>Not Recommended</p>
FE m=2		$a = 1 - b$ $b = \frac{2\zeta}{\omega_n T}$ $c = (\omega_n T)^2$	<p>Not Recommended</p>

<p>BE m=0</p>		$a = -\frac{2\zeta}{\omega_n T}$ $b = 1 - a$ $c = (\omega_n T)^2$	
<p>BE m=2</p>		$a = -\frac{2\zeta}{\omega_n T}$ $b = 1 - a$ $c = (\omega_n T)^2$	
<p>BT m=0</p>		$a = 1 - \frac{4\zeta}{\omega_n T}$ $b = 1 + \frac{4\zeta}{\omega_n T}$ $c = \left(\frac{\omega_n T}{2}\right)^2$	<p>Highly Recommended</p>
<p>BT m=2</p>		$a = 1 - \frac{4\zeta}{\omega_n T}$ $b = 1 + \frac{4\zeta}{\omega_n T}$ $c = \left(\frac{\omega_n T}{2}\right)^2$	



Description	Formula
<b>Transient Response</b> $\Delta\theta \rightarrow \theta(t)$	$\theta_{pd}(t) = \Delta\theta \exp(-\zeta\omega_n t) \left[ \cos(\omega_n \sqrt{1-\zeta^2} t) - \frac{\zeta}{\sqrt{1-\zeta^2}} \sin(\omega_n \sqrt{1-\zeta^2} t) \right]$
<b>Transient Response</b> $\Delta\theta \rightarrow f(t)$	$f_{pd}(t) = \frac{\Delta\theta\omega_n}{2\pi} \exp(-\zeta\omega_n t) \left[ \frac{2\zeta^2-1}{\sqrt{1-\zeta^2}} \sin(\omega_n \sqrt{1-\zeta^2} t) - 2\zeta \cos(\omega_n \sqrt{1-\zeta^2} t) \right]$



## Advanced Phase-Lock Techniques

James A. Crawford

2008

Artech House

510 pages, 480 figures, 1200 equations  
CD-ROM with all MATLAB scripts

ISBN-13: 978-1-59693-140-4

ISBN-10: 1-59693-140-X

Chapter	Brief Description	Pages
1	<i>Phase-Locked Systems—A High-Level Perspective</i> An expansive, multi-disciplined view of the PLL, its history, and its wide application.	26
2	<i>Design Notes</i> A compilation of design notes and formulas that are developed in details separately in the text. Includes an exhaustive list of closed-form results for the classic type-2 PLL, many of which have not been published before.	44
3	<i>Fundamental Limits</i> A detailed discussion of the many fundamental limits that PLL designers may have to be attentive to or else never achieve their lofty performance objectives, e.g., Paley-Wiener Criterion, Poisson Sum, Time-Bandwidth Product.	38
4	<i>Noise in PLL-Based Systems</i> An extensive look at noise, its sources, and its modeling in PLL systems. Includes special attention to $1/f$ noise, and the creation of custom noise sources that exhibit specific power spectral densities.	66
5	<i>System Performance</i> A detailed look at phase noise and clock-jitter, and their effects on system performance. Attention given to transmitters, receivers, and specific signaling waveforms like OFDM, M-QAM, M-PSK. Relationships between EVM and image suppression are presented for the first time. The effect of phase noise on channel capacity and channel cutoff rate are also developed.	48
6	<i>Fundamental Concepts for Continuous-Time Systems</i> A thorough examination of the classical continuous-time PLL up through 4 <sup>th</sup> -order. The powerful Haggai constant phase-margin architecture is presented along with the type-3 PLL. Pseudo-continuous PLL systems (the most common PLL type in use today) are examined rigorously. Transient response calculation methods, 9 in total, are discussed in detail.	71
7	<i>Fundamental Concepts for Sampled-Data Control Systems</i> A thorough discussion of sampling effects in continuous-time systems is developed in terms of the z-transform, and closed-form results given through 4 <sup>th</sup> -order.	32
8	<i>Fractional-N Frequency Synthesizers</i> A historic look at the fractional-N frequency synthesis method based on the U.S. patent record is first presented, followed by a thorough treatment of the concept based on $\Delta$ - $\Sigma$ methods.	54
9	<i>Oscillators</i> An exhaustive look at oscillator fundamentals, configurations, and their use in PLL systems.	62
10	<i>Clock and Data Recovery</i> Bit synchronization and clock recovery are developed in rigorous terms and compared to the theoretical performance attainable as dictated by the Cramer-Rao bound.	52